INVESTIGATION OF ATMOSPHERIC REENTRY FOR THE SPACE MANEUVER VEHICLE

THESIS

Dennis J. McNabb, Captain, USAF

AFIT/GA/ENY/04-M03

DEPARTMENT OF THE AIR FORCE
AIR UNIVERSITY

AIR FORCE INSTITUTE OF TECHNOLOGY

Wright-Patterson Air Force Base, Ohio

The views expressed in this thesis are those of the author and do not reflect the official policy or position of the United States Air Force, Department of Defense, or the U.S. Government.

AFIT/GA/ENY/04-M03

INVESTIGATION OF ATMOSPHERIC REENTRY FOR THE SPACE MANEUVER VEHICLE

THESIS

Presented to the Faculty

Department of Aeronautics and Astronautics

Graduate School of Engineering and Management

Air Force Institute of Technology

Air University

Air Education and Training Command

In Partial Fulfillment of the Requirements for the

Degree of Master of Science in Astronautical Engineering

Dennis J. McNabb, BS

Captain, USAF

March 2004

AFIT/GA/ENY/04-M03

INVESTIGATION OF ATMOSPHERIC REENTRY FOR THE SPACE MANEUVER VEHICLE

Dennis J. McNabb, BS

Captain, USAF

Approved:

_____	_____
William E. Wiesel, Civ, USAF (Chairman)	Date
_____	_____
Steven G. Tragesser, Civ, USAF (Member)	Date
_____	_____
Joerg D. Walter, Maj, USAF (Member)	Date

Abstract

This study investigated the atmospheric reentry of the Space Maneuver Vehicle from low-earth orbit using an entry guidance concept similar to the Space Shuttle. The Space Maneuver Vehicle was modeled as a point mass with aerodynamic properties as determined using Newtonian impact theory. For the rarefied-flow transition regime bridging formulae are used to capture the effects of both hypersonic continuum flow and free molecular flow. Constraints to the reentry are developed and a reentry corridor is defined in the drag-velocity plane. Bank angle modulation is established as the primary means for controlling drag and range. The guidance concept is applied to both a high inclination orbit and a low inclination orbit with crossrange requirement. Monte Carlo error analysis validates the ability of the control algorithm to guide reentry in the presence of initial state errors, as well as atmospheric variations.

Acknowledgments

I would like to express appreciation to my faculty advisor, Dr. William Wiesel, for his support and guidance throughout the course of this research effort. I would also like to thank Dr. Steven Tragesser for agreeing to teach the Atmospheric Reentry course in the Summer 2003 Quarter. The material studied in that course formed was invaluable to this research effort.

Finally, I would like to express my heartfelt appreciation to my wife for her support during my time at AFIT and throughout my career. To her I owe thanks for helping me to maintain perspective and always focus on the important things in life.

Dennis J. McNabb

.

Table of Contents

Page

Page

List of Figures

Page

Page

Page

List of Tables

Page

INVESTIGATION OF ATMOSPHERIC REENTRY FOR THE SPACE MANEUVER VEHICLE

I. Introduction

Background

Over the last decade, the importance of space assets to the warfighter has been demonstrated through various regional conflicts. The ability to communicate with troops in the field, predict weather conditions, and monitor the enemy's movements from space all combine to give theater commanders an unprecedented battlefield awareness. Over the next few decades control of the high ground of space will play an even more crucial role in regional, as well as global, conflicts.

At the current time, launching payloads into space is a lengthy process sometimes taking years to complete. Additionally, the combined cost of the satellite and launch vehicle is typically in the hundreds of millions of dollars range. Not surprisingly, "routine, reliable, and lower-cost space operations are goals of U.S military planners" (Shaw, 2000:1). One concept from the Air Force Space Command (AFSPC) Strategic Master Plan proposed to meet these goals is the Military Spaceplane (MSP) (Shaw, 2000:1). The MSP consists of four primary components (Shaw, 2000:1):

- Space Operations Vehicle (SOV): a reusable launch element to reduce the cost of, improve the flexibility of, and increase the responsiveness of earth-to-orbit operations;

- Space Maneuver Vehicle (SMV): an uncrewed, reusable satellite bus and upper stage with significant maneuvering capability;
- Modular Insertion Stage (MIS): a low cost expendable upper stage to reduce the cost and improve the operability of Space Support missions;
- Common Aero Vehicle (CAV): an aeroshell designed to deliver material (e.g. munitions, UAVs, or critical supplies) through space directly to a theater.

For this study, the SMV component of the MSP is of primary concern. The SMV is envisioned to have between 7000 and 12000 fps of ΔV--approximately 100 times the maneuvering capability of current satellites (Shaw, 2000:6). The maneuvering capability combined with the intended mission duration of less than 12 months (on the order of weeks for tactical missions) allows the SMV to perform significant orbital maneuvers to accomplish the intended mission. For reference, in a medium altitude earth orbit a ΔV of 10000 fps will allow for a 20°-plane change (Shaw, 2000:7). In addition to on orbit maneuverability, the SMV is intended to be responsive to the needs of the warfighter. The goal is for "warfighers [to] have tailored satellite-based services soon after they requested them" (Shaw, 2000:7).

A Military Utility Analysis (MUA) conducted during 1998 and 1999 showed that the capabilities of the SMV would most likely be used for force enhancement, space control, and space test in the near future (Shaw, 2000:9-10). Comparison of the SMV capabilities against the Air Force Space Command Strategic Master Plan (SMP) for 2000 shows the SMV will have a "direct and substantial" effect on 4 of the top 10 priorities in the near-term, and 6 of the top 10 priorities in the mid-term (Shaw, 2000:11). According to the Air Force Research Lab's Space Vehicles Directorate (AFRL/SV) the SMV could perform the following classes of missions (AFRL 2004):

- Intelligence, surveillance and reconnaissance of ground targets (with either integrated or deployable ISR satellite)
- Deployment and recovery of microsatellites (e.g. Space Control Satellites)
- Rapid constellation replenishment

Currently there are two technology programs being worked to demonstrate the feasibility of the SMV concept. These two programs are the Boeing and US Air Force X-40A and the NASA and Boeing X-37 (Shaw, 2000:17). The Air Force is also contributing funds to the X-37 program to demonstrate technologies for future reusable military spacecraft (Shaw, 2000:17).

The Air Force X-40A (22 feet long and weighs about 2600 lb) is a test vehicle designed to evaluate the low speed atmospheric flight dynamics of the X-37 (Dryden 2004). The X-40A, shown if Figure 1, successfully completed its series of seven test

Figure 1: X-40A Space Maneuver Vehicle (Dryden 2004)

flights at NASA Dryden Research Center where it autonomously acquired the runway and executed an aircraft landing after being dropped from an Army Chinook helicopter at 15,000 ft (X-37 2004). The X-40A is often referred to as the X-40A Space Maneuver Vehicle, however, it is a technology demonstrator for the Space Maneuver Vehicle concept. For the purposes of this study, the fully operational SMV will be considered, not the X-40A.

The X-37 (shown in Figure 2) is being designed to operate on orbit as well as during the reentry phase of flight. The X-37 is capable of fitting into the Space Shuttle payload bay for launch into orbit, or it can be carried to orbit by an expendable launch vehicle (Marshall 2004). Technologies that will be demonstrated by the X-37 include: advanced airframe design, avionics technologies, and advanced thermal protection systems (Marshall 2004).

Figure 2: X-37 Reusable Spaceplane (Marshall 2004)

The goal of the current study is to develop an entry guidance algorithm capable of guiding an operational Space Maneuver Vehicle through atmospheric reentry to a pre-determined termination point in the vicinity of the runway. The currently operational Space Transportation Systems (STS) Space Shuttle Orbiters are an obvious starting point for developing the guidance algorithm. The Space Shuttle has been operational since 1981 and has demonstrated the capability of its reentry guidance system on over 100 landings. Therefore, this study will focus on applying the concepts used in Space Shuttle entry guidance to the Space Maneuver Vehicle.

Space Shuttle entry guidance is "designed on the principal of analytically defining a desired drag acceleration profile and commanding the orbiter to achieve the desired profile" (Harpold & Graves, 1978:103). Thus, the guidance approach employed is to establish the reentry corridor in the drag-velocity (D-V) plane by defining the constraints, define a desired drag acceleration profile in the D-V plane, and then command the vehicle to fly on the defined profile. The primary control variable used during the entry phase is the bank angle, ϕ. The bank angle is modulated to control both the drag acceleration level and the range to the termination point.

In order to apply the shuttle entry guidance concept to the SMV, the reentry problem must first be setup. This is the focus of Chapter 2. In Chapter 2, the equations of motion governing a point-mass vehicle reentering the Earth's atmosphere are developed. Next, since the SMV exists in concept only, its aerodynamic properties are derived.

Having defined the problem and the aerodynamic properties of the vehicle in Chapter 2, Chapter 3 develops the guidance algorithm. First the initial and final conditions for the reentry trajectory are developed. Next, the entry corridor is defined by deriving the constraints in the D-V plane. A reference profile in the D-V plane is then developed. With the reference profile within the entry corridor established, the control law and guidance algorithm which will guide the vehicle during its descent are developed.

Chapter 4 examines two scenarios of the SMV reentering the Earth's atmosphere with the Shuttle entry guidance concept applied. Results are presented which show the entry profile within the D-V plane, as well as the bank angle and angle of attack profiles. Additionally, the ground track of the reentry path and a plot of azimuth angle show the effects of the roll-reversal commands within the guidance algorithm. Finally, a 100-run Monte Carlo error analysis simulation is run to examine the performance of the developed guidance system in the presence of errors in the initial state, aerodynamics, and atmosphere.

Chapter 5 then summarizes the results of applying the concepts of Shuttle entry guidance to the Space Maneuver Vehicle. The results are interpreted to show the success of the entry guidance algorithm. Areas of improvement within the design are noted, and recommendations are made for future areas of study.

As a final note, the author wishes to point out that the units used within this study are often mixed. For the majority of the study the SI system of units is employed. However, it is standard in the literature of the subject to use units of feet per second (fps)

for velocity, feet (ft) for altitude, and nautical miles (nmi) for distance. Where appropriate these units will be given in addition to the SI units.

II. Problem Setup

Chapter Overview

The purpose of this chapter is to set up the atmospheric reentry problem for the Space Maneuver Vehicle (SMV). First, the equations of motion for a point mass reentering the Earth's atmosphere will be stated. Next, a model of the Space Maneuver Vehicle will be constructed. Using the model the aerodynamic properties of the reentry vehicle will be approximated using Newtonian impact theory. Finally, assumptions will be made concerning the Earth's atmosphere and gravitational field.

Equations of Motion

The first step in examining a body reentering the Earth's atmosphere is to develop a set of equations to describe the motion. The set of equations developed and used herein is similar to the set used in Vinh as well as in Regan and Anandakrishnan. The differences are that the flight path angle, γ, will be positive below the horizontal plane, and the heading angle, ψ, will be measured from North, instead of East.

The coordinate system used is constructed with one axis aligned with the Earth-relative velocity vector (Harpold and Graves, 1978:106). The position of the vehicle is defined by a vector from the center of the Earth to the vehicle. Then, the plane formed by this vector and the velocity vector is perpendicular to the second axis, with the third axis completing the right-handed coordinate system (Harpold and Graves, 1978:106). The equations or motion developed in this coordinate system are:

$$\dot{V} = -D + g\sin\gamma \tag{1}$$

$$V\dot{\gamma} = \left(g - \frac{V^2}{r}\right)\cos\gamma - L\cos\phi \tag{2}$$

$$V\cos\gamma\dot{\psi} = \left(\frac{V^2}{r}\right)\cos^2\gamma\sin\psi\tan\theta - L\sin\phi \tag{3}$$

where:

V = Earth-relative velocity (km/s)

D = Drag (km/s^2)

g = Gravitational acceleration (km/s^2)

γ = Flight path angle

r = (Re + h) (km)

Re = Radius of Earth (km)

h = Altitude of vehicle (km)

L = Lift (km/s^2)

ϕ = Bank angle

ψ = Heading angle

θ = Latitude

The derivation of these equations is presented in *Hypersonic and Planetary Entry Flight Mechanics* and is not duplicated herein (Vinh, 1980:21-27). It is worth noting, however, that certain assumptions have been employed to simplify the equations to the form presented above. Assuming a non-rotating Earth, and therefore a non-rotating atmosphere, eliminates the ω and ω^2 terms which result due to the Earth's rotation (Vinh,

1980:27). In other words, the Coriolis and centripetal acceleration have been neglected. This assumption is appropriate since the effects of the rotating atmosphere on the vehicle are small compared with aerodynamic forces due to the vehicle's velocity (Vinh, 1980:3). This approach is consistent with the methods used in *Shuttle Entry Guidance* (Harpold & Graves, 1978:106).

Figure 3 shows the coordinate system employed in this analysis. For the purposes

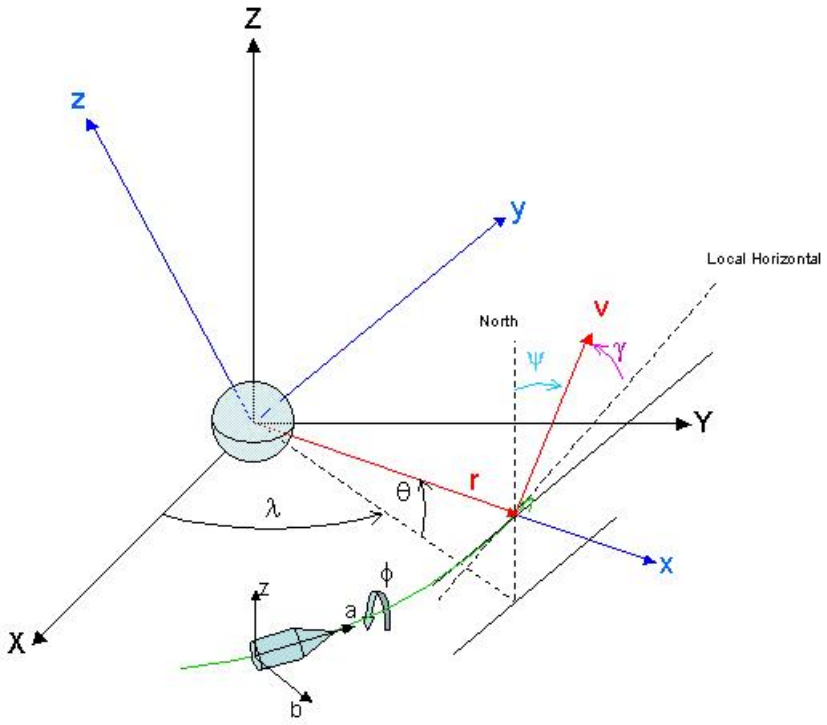

Figure 3: Reentry Coordinate System

of this study the vehicle is considered to be a point mass. The bank angle, ϕ, is defined as positive in the right-handed sense about the drag vector (ie. opposite the velocity vector).

That is, referencing Figure 3, positive roll is defined as roll to the left, and negative roll as roll to the right. The heading angle, ψ, is measured clockwise from North to the velocity vector.

The set of equations presented (Eqns. 1-3) are the kinetic equations of motion for this system. To completely describe the system, the kinematic equations must also be understood. Once again, the equations used in this study are similar to those derived in *Hypersonic and Planetary Flight Mechanics* (Vinh, 1980:26). The kinematic equations are:

$$\dot{h} = -V \sin\gamma \tag{4}$$

$$\dot{\theta} = \frac{V \cos\gamma \sin\psi}{r \cos\phi} \tag{5}$$

$$\dot{\lambda} = \frac{V \cos\gamma \cos\psi}{r} \tag{6}$$

where λ = Longitude.

Vehicle Model

The equations developed in the preceding section act to model the dynamics of atmospheric reentry. The purpose of this study is to examine the dynamics of a particular lifting-body reentry vehicle—the Space Maneuver Vehicle. At present, the SMV exists in concept only, however, the X-40A and X-37 programs are actively developing technologies in support of its development (Shaw, 2000:1). What does exist for the SMV is nominal values for vehicle parameters ranging from weight, to length, to payload bay dimensions (Shaw, 2000:2).

In order to study the reentry characteristics of a given vehicle, an aerodynamic model of the vehicle must be developed. The approach taken in this study is to build a model of the Boeing SMV concept in MATLAB and use the model to determine the aerodynamic characteristics using Newtonian impact theory. Table 1 below presents the dimensions of the SMV taken from the Boeing SMV concept:

Table 1: SMV Parameters (Shaw, 2000:2)

Parameter	Value
Weight	10000 lb
Length	29 ft
Wingspan	15 ft
Height	9.5 ft

In addition to the parameters presented in Table 1, dimensions including nose width, body width, and chord length were determined based on interpretation of Boeing X-37 concept drawings (Figure 4).

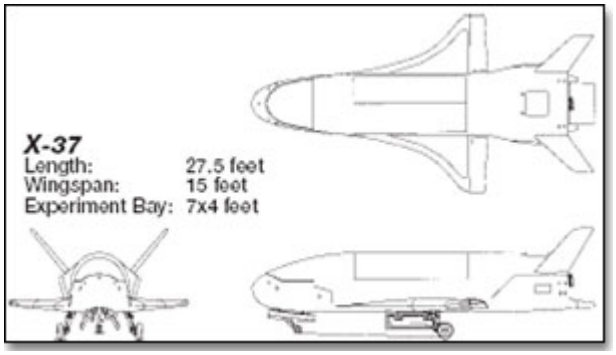

Figure 4: Boeing X-37 (X-37 2004)

These values were then used to create a 60-panel model of the SMV using MATLAB, see Figure 5. A more detailed diagram is shown in Appendix A.

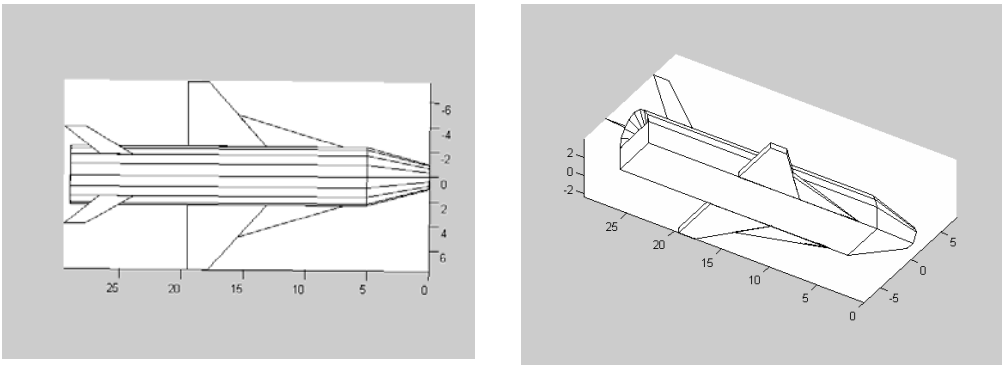

Figure 5: MATLAB model of Space Maneuver Vehicle

The model was then used to determine the forces acting on the vehicle through the employment of Newtonian impact methods. Newtonian impact theory assumes that a particle of fluid which impinges upon a body will lose all momentum normal to the surface, while the tangential momentum will be unaffected (Regan, 1993:352). This method can be employed to determine the forces acting on a flat plate (or in the case of the vehicle model, a series of flat plates) in both the free-molecular flow and hypersonic continuum regions (Regan, 1993:356). The FORTAN code used for this analysis was provided by Dr. William Wiesel, Professor of Astronautical Engineering, AFIT, and is similar to the code provided in *Dynamics of Atmospheric Reentry* (Regan, 1993:321-328).

Aerodynamic Properties.

Upon returning from orbit the vehicle will pass from the near vacuum conditions of space, through the upper regions of Earth's atmosphere, to the denser regions of the lower atmosphere. Throughout the reentry trajectory the vehicle will be operating in one of three flight regimes: free molecular flow, transition, or continuum flow (Regan, 1993:316). The regime that the vehicle is operating in is dependent upon the Knudsen number. The Knudsen number is a non-dimensional parameter which indicates the relative importance of the particulate nature of air (Regan, 1993:316). The Knudsen number can be defined as (Regan, 1993:316):

$$Kn = \frac{\lambda}{L} = \frac{mean\ free\ path}{characteristic\ length} \tag{8}$$

The mean free path of a particle is a measure of the relaxation distance in a gas (Regan, 1993:316). The relaxation distance is a measure of the distance a particle of gas will move through a flowfield before interacting with another particle of gas (Regan, 1993:313). If the flowfield has a high number density of particles then the collision frequency will be high and this distance will be short (Regan, 1993:313). In this case, the flowfield can be treated as a continuum. In contrast, in a region where the number density of particles is low, the collisions will occur less frequently and the relaxation distance will be longer (Regan, 1993:314). In this case the flowfield can be treated as free molecular flow. The characteristic length is typically chosen as the mean aerodynamic chord (MAC) for a lifting body.

It now remains to define what is meant by short and long relaxation distances. The free molecular flow region is defined as the region where Kn >> 1, while the

continuum region is defined where Kn << 1 (Regan, 1993:316). For the purposes of this study, regions where Kn > 10 will be considered free molecular flow regions. For the region where Kn < .01, the flowfield will be treated as a continuum. The region between the two, .01 ≤ Kn ≤ 10 will be considered the rarefied-flow transition region (Blanchard, 1994:550). In this region the flow cannot be treated as a continuum, nor can the particulate nature of the gas molecules be neglected. In this region, the following empirical bridging formula will be used (Blanchard, 1994:553):

$$\overline{C}_N = \exp[-0.29981(1.3849 - \log_{10} Kn)^{1.7128}] \quad (9)$$

$$if\ \log_{10} Kn < 1.3849$$

$$otherwise\ \overline{C}_N = 1.0$$

$$\overline{C}_A = \exp[-0.2262(1.2042 - \log_{10} Kn)^{1.8410}] \quad (10)$$

$$if\ \log_{10} Kn < 1.2042$$

$$otherwise\ \overline{C_A} = 1.0$$

where $\overline{C}_N$ and $\overline{C}_A$ are the bridging coefficients, with values between 0 and 1. These coefficients are then used to bridge the transition region as follows:

$$C_N = C_{N_C} + (C_{N_F} - C_{N_C})\overline{C_N} \quad (11)$$

$$C_A = C_{A_C} + (C_{A_F} - C_{A_C})\overline{C_A} \quad (12)$$

where:

C_N = Normal aerodynamic force coefficient

C_A = Axial aerodynamic force coefficient

and the subscripts "*F*" and "*C*" denote the free molecular flow and continuum regions, respectively.

For a given reentry vehicle, and therefore a given characteristic length, the Knudsen number as a function of altitude can be determined. The Knudsen number can be represented as (Regan, 1993:315):

$$Kn = \frac{m / (\sqrt{2}\pi\sigma^2\rho_0 e^{-h/H})}{L} \tag{13}$$

where:

m = particle mass (kg)

σ = effective diameter of gas particles (km)

ρ_0 = earth surface density (kg/km^3)

H = scale height (km)

Figure 6 is plot of Knudsen Number as a function of altitude, with the mean aerodynamic

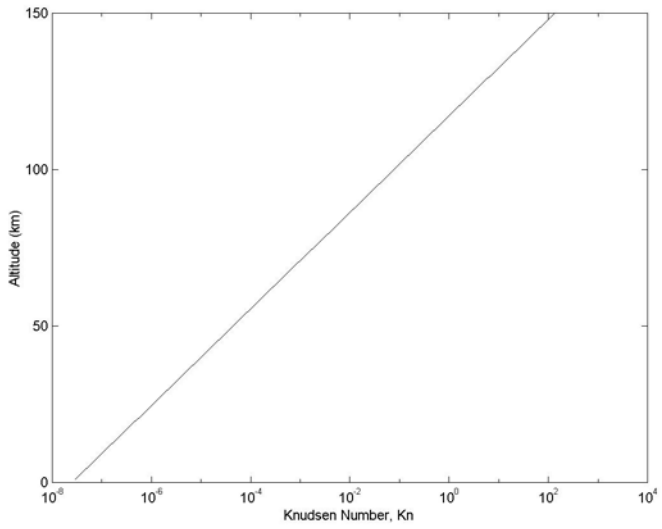

Figure 6: Altitude vs. Knudsen number, MAC=5.85ft

chord (MAC=5.85 ft) calculated from the MATLAB model of the SMV. Therefore, the transition region from free molecular flow to hypersonic continuum flow is from approximately 130 km to 70 km altitude. For the purposes of this study, reentry begins at 400,000 ft altitude, or approximately 122.2 km. Therefore, the vehicle will begin reentry in the transition region and enter the continuum region at approximately 70 km.

To this point, a flat-panel model of the vehicle has been created and a method for accounting for the particulate nature of the flow-field has been developed. The goal is to determine the aerodynamic coefficients of the reentry vehicle for use in the equations of motion and the guidance algorithm. In particular, a polynomial function of angle of attack, α, is desired. From the aforementioned Newtonian impact theory analysis the lift and drag coefficients as functions of angle of attack for both the free molecular flow region and the hypersonic continuum flow region have been developed. The resulting lift coefficients are shown in Figures 7 and 8.

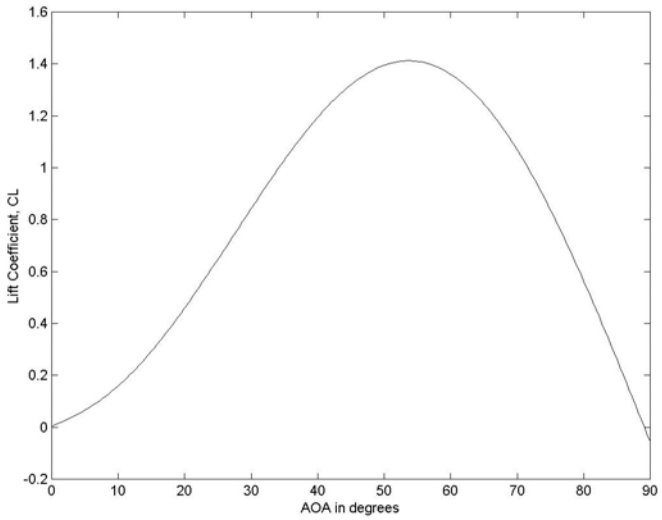

Figure 7: Hypersonic Continuum Lift Coefficient

Figure 8 shows the expected result that very little lift is being generated in the free molecular flow region.

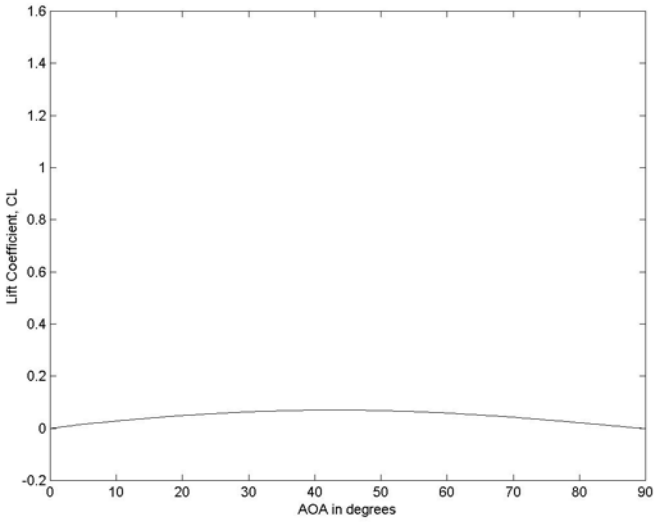

Figure 8: Free Molecular Flow Lift Coefficient

Figures 9 and 10 show the determined drag coefficients in the hypersonic continuum and free molecular flow regions, respectively.

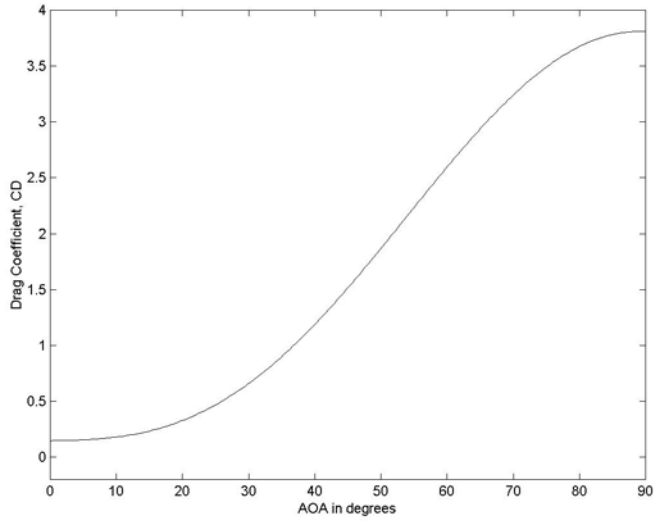

Figure 9: Hypersonic Continuum Drag Coefficient

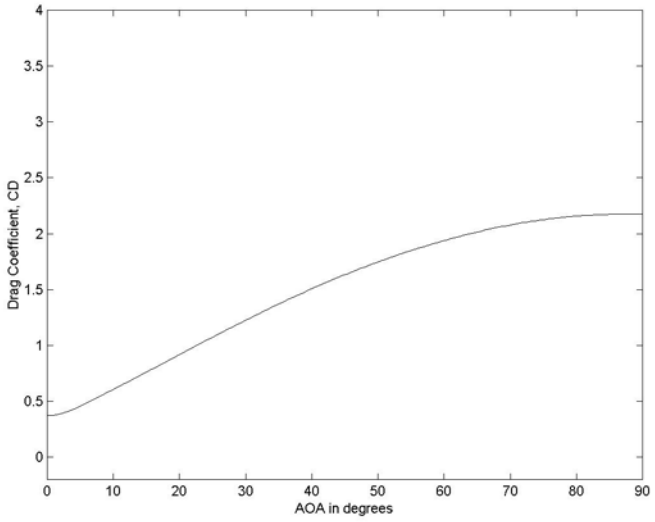

Figure 10: Free Molecular Flow Drag Coefficient

To determine polynomial expressions for the aerodynamic coefficients in each region, a least squares method was employed. First, it was determined that a quadratic expression of the aerodynamic coefficient in terms of angle of attack would be used. Next, since reentry at a high angle of attack is desirable to minimize aerodynamic heating, the range of angle of attack over which the vehicle would operate during reentry was established as 15°-50° (Chapman, 1967:37). For each case (ie. lift coefficient in the continuum region), this defined an over-determined set of equations in three unknowns. This system of equations can be expressed as:

$$[A]\bar{x} = \bar{b}_{LC} \tag{14}$$

The matrix $[A]$ has three columns. The first column is the square of the angle of attack, the second column is the angle of attack, and the third column is 1. Thus:

$$[A] = \begin{pmatrix} AOA_1^{\,2} & AOA_1 & 1 \\ \vdots & \vdots & \vdots \\ AOA_n^{\,2} & AOA_n & 1 \end{pmatrix} \tag{15}$$

The elements of the vector $\bar{b}_{LC}$ are the lift coefficients in the hypersonic continuum region corresponding to the particular angle of attack. Thus:

$$\overline{b_{LC}} = \begin{bmatrix} C_{LC1} \\ \vdots \\ C_{LCn} \end{bmatrix} \tag{16}$$

Since the system of equations is overdetermined, it is unlikely that there will be a solution, $\bar{x}$, which exactly fits the data in $\overline{b_{LC}}$. The least squares solution to an overdetermined system such as this satisfies:

$$[A]^T [A] \overline{X} = [A]^T \bar{b}_{LC} \tag{17}$$

where the vector, $\overline{X}$, contains the coefficients of the quadratic (Strang, 1988:156):

$$a(AOA_i)^2 + b(AOA_i) + c = C_{LCi} \tag{18}$$

Since the columns of the matrix $[A]$ are linearly independent, the matrix $[A]^T [A]$ is invertible, and the solution to the least squares problem can be written as (Strang, 1988:156):

$$\overline{X} = ([A]^T [A])^{-1} [A]^T \bar{b}_{LC} \tag{19}$$

Then, solving for the coefficients, the lift coefficient in the hypersonic continuum flight regime is approximated by:

$$C_{LC} = -3.3069 * 10^{-4} (AOA)^2 + 0.0552(AOA) - 0.5034 \tag{20}$$

The preceding procedure is repeated to determine the lift coefficient in the free-molecular flow region simply by replacing the vector, $\bar{b}_{LC}$, with the vector, $\bar{b}_{LF}$, which is made up of the lift coefficients in the free molecular flow region. Then the lift coefficient in the free molecular flow region is approximated by:

$$C_{LF} = -3.8241*10^{-5}(AOA)^2 + 0.0033(AOA) - 0.0022 \quad (21)$$

Figures 11 and 12 show the polynomial approximation of the lift coefficients over the region of interest in the hypersonic continuum region and the free molecular flow region, respectively.

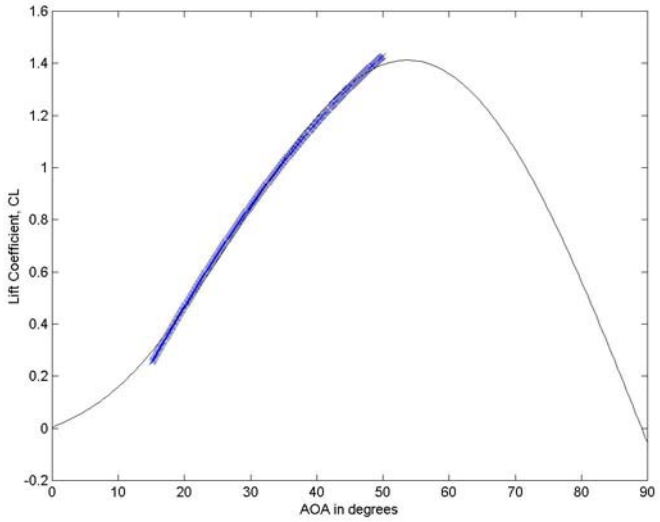

Figure 11: Quadratic Expression of Hypersonic Continuum Lift Coefficient

The drag coefficients in each region of flight are determined by the same procedure outlined above. The resulting polynomial approximations of the drag coefficients are:

$$C_{DC} = -9.6602*10^{-4}(AOA)^2 - 0.0150(AOA) + 0.2402 \quad (22)$$

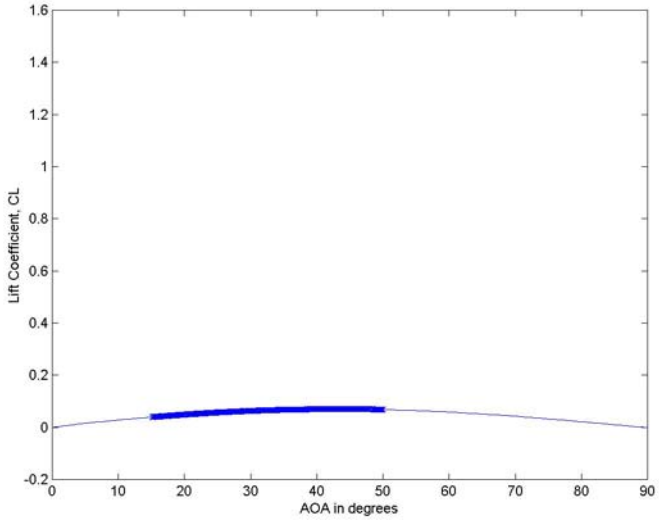

Figure 12: Quadratic Expression of Free Molecular Flow Lift Coefficient

for the hypersonic continuum region, and

$$C_{DF} = -1.3241*10^{-4}(AOA)^2 + 0.0373(AOA) + 0.2265 \tag{23}$$

for the free molecular flow region. Figures 13 and 14 show the polynomial

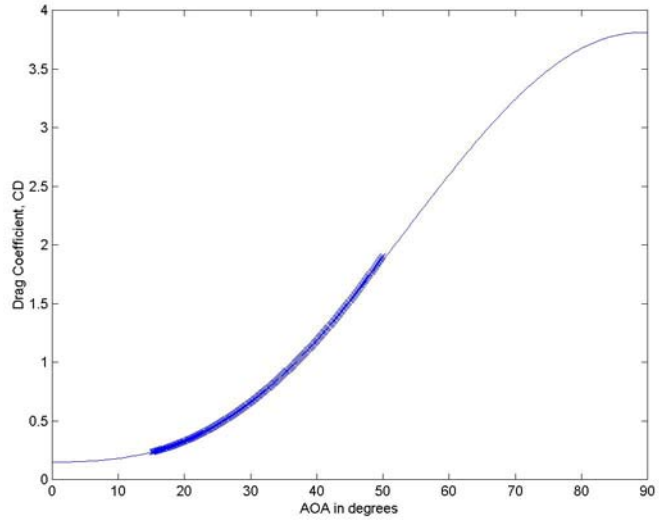

Figure 13: Quadratic Expression of Hypersonic Continuum Drag Coefficient

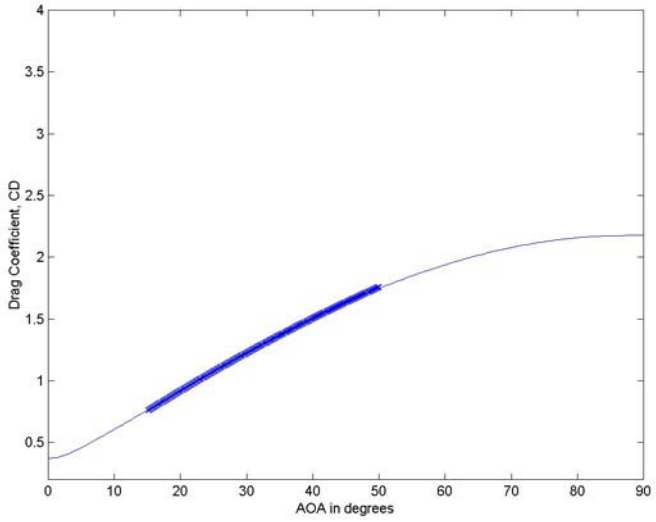

Figure 14: Quadratic Expression of Free Molecular Flow Drag Coefficient

approximations to the drag coefficients in the hypersonic continuum and free molecular regions, respectively.

Physical Assumptions

For this analysis the gravitational field of the earth is assumed to be constant. That is, the magnitude of the gravitational force is independent of altitude and position. The atmosphere is modeled as an exponential atmosphere described by (Regan, 1993:38):

$$\rho = \rho_0 \exp(-h/H) \tag{24}$$

where:

ρ_0 = sea-level density (1.752*10^9 kg/km^3)

H = Scale height (6.7 km)

This atmospheric model shows excellent agreement with the 1976 Standard Atmosphere to an altitude of approximately 120 km (Regan, 1993:39).

III. Methodology

Chapter Overview

The purpose of this chapter is to develop the guidance approach that will be used to guide the SMV during reentry. First, a set of initial and final conditions which bound the trajectory will be developed. Next, the concept of drag profile guidance will be developed and applied to this particular vehicle. Finally, the guidance and control algorithms will be developed.

Boundary Values

The guidance approach used will guide the reentry vehicle from the conditions at an initial state to the conditions at a final state without violating any reentry constraints. In this section, the initial and final conditions will be developed.

In a somewhat counter-intuitive approach, the final conditions will first be developed, and then the initial conditions. This approach is driven by the fact that a key element of a successful reentry is that the vehicle reaches the desired termination point at an acceptable energy state. Therefore, the final position is fixed to ensure this condition is met, and then the initial conditions are determined based upon range constraints.

The reentry guidance for the Space Shuttle is designed to "control the entry trajectory from initial penetration of the Earth's atmosphere (altitude of 400,000 ft and range of approximately 4100 nmi from runway) until activation of the terminal area guidance at an Earth-relative speed of 2500 fps" (Harpold and Graves, 1978:99). This

paper will not explore the guidance that controls the vehicle to the runway from the termination point.

To determine the location of the termination point, the value of Earth-relative velocity of 2500 fps (0.764 km/s) used for the Space Shuttle will be used as the terminating velocity. The altitude at termination of entry guidance will be 29.4 km (96,250 ft) and the distance from the termination point to the runway will be 30 km (16.1 nmi). The range that the vehicle is capable of flying from this point can be estimated by (Harpold and Graves, 1978:109):

$$R = \frac{(E_F - E_G)}{(D_F - D_G)} \ln \frac{D_F}{D_G} \tag{25}$$

where:

E_F = specific energy at termination point (km^2/s^2)

E_G = specific energy at landing (km^2/s^2)

D_F = drag at termination point (km/s^2)

D_G = drag at landing (km/s^2)

With the values above for termination velocity and altitude, and a landing speed of 250 fps, the remaining range of the vehicle is approximately 64 km (34.5 nmi). This excess energy would either be dumped through wide turns or used to align the vehicle with the runway. An alternate method of predicting the range to go from the termination point based upon integration of the equations of motion is presented in Appendix B. The two methods show agreement, with the method presented herein being the more conservative.

By defining the entry guidance termination values for velocity and altitude, the terminal value for drag is also defined, since;

$$D = \frac{1}{2}\rho V^2 C_D S \tag{26}$$

and the angle of attack at termination, and therefore the drag coefficient, is specified.

Next, the physical location on the Earth of the entry guidance termination point will be determined. For this paper, the landing site is assumed to be at Kennedy Space Center (KSC), FL. The coordinates of KSC are:

Latitude: 28.6° N

Longitude: 279.4° E

The entry guidance termination point will be determined to lie 30 km directly West of KSC. Since one degree of longitude (°L) is:

$$°L = 2\pi R_e \cos(Latitude)/360$$

the coordinates of the entry guidance termination point are:

Latitude: 28.6° N

Longitude: 279.1° E

Table 2 summarizes the conditions at entry guidance termination:

Table 2: Terminal Conditions for Entry Guidance

Conditions	**Value**
Velocity	0.764 km/s
Altitude	29.4 km
Latitude	28.6° N
Longitude	279.1° E

Next, the initial conditions for the reentry trajectory must be determined. The reentry trajectory will begin at an altitude of 122.2 km (400,000 ft)—the same altitude used for Shuttle entry guidance (Harpold and Graves, 1978:99). The velocity at reentry will be dependent upon the altitude of the vehicle orbit. For this study, the initial orbit of the vehicle will be assumed circular. The de-orbit burn will be the first burn of a Hohmann transfer from the initial orbit to a circular orbit of 80 km, as illustrated in Figure 15.

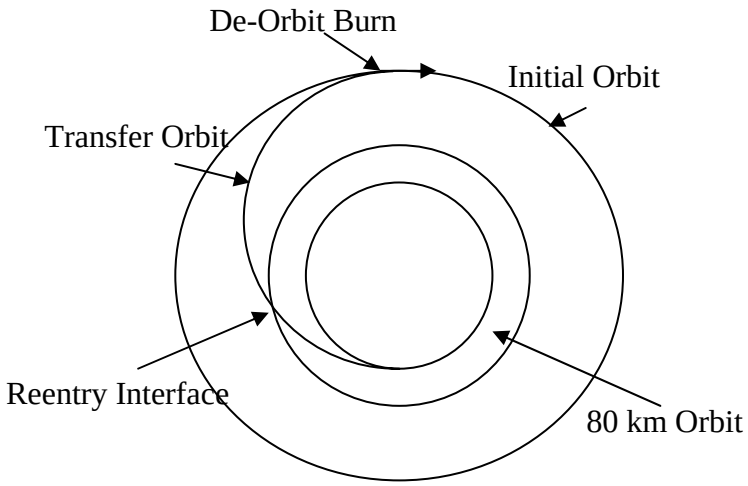

Figure 15: De-Orbit and Reentry Interface

For the transfer ellipse (Wiesel, 1997:56):

$$a_t = \frac{a_i + a_f}{2} \tag{27}$$

and

$$r_p = a_t(1-e) \tag{28}$$

where r_p is the perigee point of the transfer ellipse, e is the eccentricity and:

a_t = semi-major axis of transfer ellipse (km)

a_i = semi-major axis (radius) of initial orbit (km)

a_f = semi-major axis (radius) of 80 km destination orbit

The equations above can be solved to find the semi-major axis and eccentricity of the transfer ellipse. These quantities can then be used to determine the magnitude of the angular momentum, h, from (Wiesel, 1997:56):

$$h = \sqrt{\mu a(1-e^2)} \tag{29}$$

Then, letting r be equal to the distance from the center of the Earth to the vehicle at the reentry altitude (ie. r = Re + 122.2 km), the initial velocity can be found from (Wiesel, 1997:74):

$$V_0 = \sqrt{\mu(\frac{2}{r} - \frac{1}{a})} \tag{30}$$

Then the initial flight path angle, γ_0, can be determined from (South, 1974:159):

$$\gamma_0 = \cos^{-1}\frac{h}{rV_0} \tag{31}$$

The preceding equations have specified the initial energy state for the reentry vehicle. Now the location of the vehicle at the beginning of the reentry trajectory, with respect to a non-rotating earth, must be determined. The position of the vehicle at the initiation of the reentry trajectory will be a function of the projected range of the vehicle. This projected range, in turn, will be a function of the vehicle's initial velocity, pre-determined drag profile, and terminal conditions. The drag profile which the vehicle will follow will be developed in the next section. As such, further discussion of the position of the vehicle at reentry is presented in Appendix C. The initial conditions for reentry from an initial circular orbit of 500 km are summarized in Table 3.

Table 3: Initial Conditions for Entry Guidance (h_0=500km)

Conditions	Value
Velocity	7.940 km/s
Altitude	122.2 km
Latitude	Orbit Dependent
Longitude	Orbit Dependent

Drag Profile Guidance

This section will develop the concept of controlling the vehicle's reentry trajectory by controlling to a desired drag profile. First the concept of the drag-velocity (D-V) plane and the limiting constraints will be developed. Next, a three-phase nominal reentry profile will be developed in the drag-velocity plane.

Reentry Constraints.

For a vehicle reentering the Earth's atmosphere there are four primary constraints that determine the reentry corridor. For the purposes of this study, these constraints will be plotted in the D-V plane. During the early phase of entry the vehicle will be subjected to high heating rates as it descends into the increasingly dense atmosphere. While heating rates are the primary concern during the early phase of reentry, later in flight vehicle normal loads and dynamic pressure loads become increasingly important. The final constraint is the range constraint. A functional guidance program will guide a vehicle through the reentry corridor without violating the physical constraints while delivering the vehicle to a pre-determined termination point at an acceptable energy state.

Heating Rate.

For a vehicle reentering the earth's atmosphere two heat related quantities must be accounted for: heating rate and heating load. For a vehicle that uses an ablation type heat shield, the total heat load, or heat absorbed, is of primary importance (Chapman, 1967:38). For a radiation-cooled vehicle the maximum heating rate is the driving factor (Chapman, 1967:38). As mentioned earlier, the SMV exists only in concept at this point, however, the Boeing X-37 will test possible thermal protection system (TPS) materials which could be used on an operational SMV (Shaw 2000:114). Therefore, for the purposes of this study, the assumption will be made that the SMV reentry heating constraint will be controlled by the heating rate.

The heating rate constraint equation is (Lu, 1997:145):

$$\sqrt{\frac{\rho}{\rho_{0,ref}}}\left[\frac{\sqrt{R_e g_0}}{v_{ref}}\right]^3\left[\frac{V}{\sqrt{R_e g_0}}\right]^3 \le \frac{\dot{q}_{\max}}{C_q} \tag{32}$$

where:

$\rho_{0,ref}$ = 1 kg/m^3

v_{ref} = 1 m/s

$\dot{q}_{\max}$ = maximum stagnation point heating rate (W/m^2)

C_q = heat flux transmission coefficient (W/m^2)

The parameters for maximum stagnation point heating rate ($\dot{q}_{\max}$) and heat flux transmission coefficient (C_q) are taken from Lu for a reusable launch vehicle (RLV) and based on a reference sphere of 1m (Lu, 1997:145):

$\dot{q}_{\max}$ = 544,300 W/m^2

$C_q = 1.65*10^{-4}$ W/m^2

Then, Equation (32) can be rearranged to yield:

$$\rho V^2 = \frac{\rho_{0,ref} v_{ref}^{\ 6} \dot{q}_{\max}^{\ 2}}{C_q^{\ 2} V^4} \tag{33}$$

This expression can then be substituted into the drag equation to give:

$$\frac{D}{m} = \frac{1}{2m} C_D S \frac{\rho_0 v_{ref}^{\ 6} \dot{q}_{\max}^{\ 2}}{C_q^{\ 2} V^4} \tag{34}$$

All that remains to do to quantify the heating constraint is to specify the angle of attack profile. The angle of attack profile is chosen such that the reentry vehicle initially enters the atmosphere with a high angle of attack and maintains that angle of attack until a specified velocity. At the specified velocity, the angle of attack will decrease linearly to the angle of attack corresponding to max L/D at the final conditions. Figure 16 shows the angle of attack profile used in this study for the SMV.

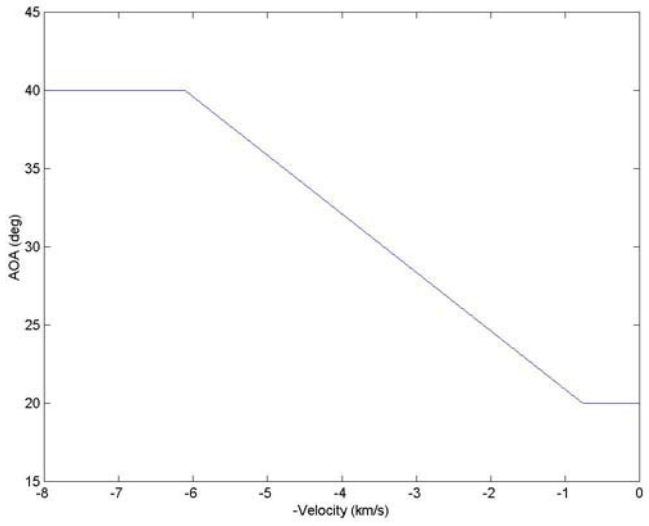

Figure 16: Angle of Attack profile

Using the angle of attack profile, the drag per unit mass can be plotted versus velocity as shown in Figure 17.

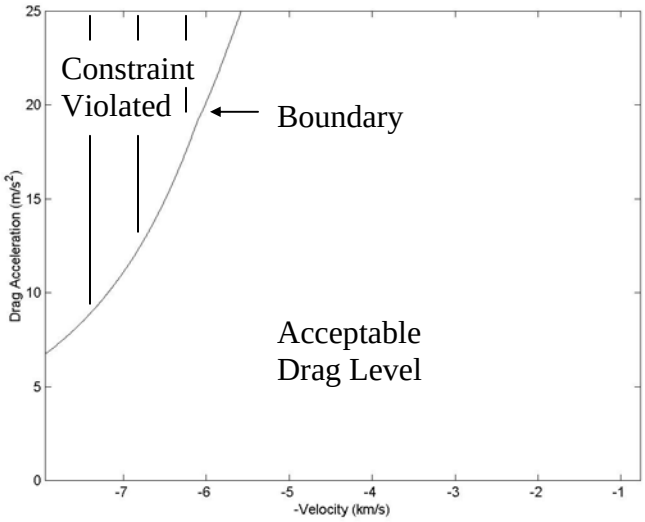

Figure 17: Heating Constraint in D-V Plane

It should be noted that drag is plotted against negative velocity as a convention. In the D-V plane the vehicle will be traveling from left to right as it enters the atmosphere and decelerates to its terminal point. The heating constraint represents the first constraint to reentry—developing the other constraints will develop the reentry corridor.

Maximum Normal Load.

The maximum normal load constraint represents the maximum load constraint in the body-normal direction (Lu, 1997:145). Figure 18 shows the relationship of the forces acting on a reentry body:

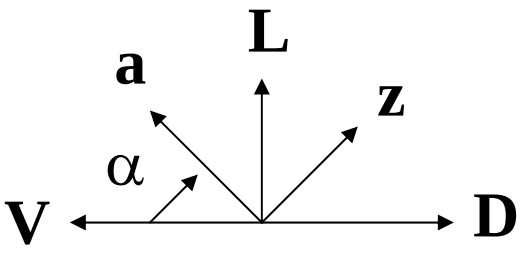

Figure 18: Aerodynamic Forces on Reentry Vehicle

In the above figure, **z** represents the body normal axis, and **a** represents the longitudinal axis of the vehicle. As can be seen from the figure, both lift and drag contribute to the normal loads on the vehicle. From the geometry it can be seen that the normal load on the vehicle is:

$$\overline{N}_Z = \frac{L}{m}\cos\alpha + \frac{D}{m}\sin\alpha \tag{35}$$

Substitute,

$$L = \frac{L}{D}D = \frac{C_L}{C_D}D \tag{36}$$

then,

$$\overline{N}_Z = \frac{C_L}{C_D}\frac{D}{m}\cos\alpha + \frac{D}{m}\sin\alpha \tag{37}$$

Let the maximum normal load constraint be $\overline{N}_{Z,\max}$. Then, rearrange and solve for D/m:

$$\frac{D}{m} \le \frac{\overline{N}_{Z,\max}}{\frac{C_L}{C_D}\cos\alpha + \sin\alpha} \tag{38}$$

From Harpold and Graves, the maximum normal load boundary for the Space Shuttle is defined to be 2.5g (1978:103). Therefore, setting $\overline{N}_{Z,\max}$ = 2.5g and plotting in the D-V plane yields the normal load constraint as shown in Figure 19.

Dynamic Pressure Constraint.

The dynamic pressure constraint to reentry can be seen directly from the drag equation. Letting q_{max} be the maximum allowable dynamic pressure leads directly to:

$$\frac{D}{m} \leq q_{\max} \frac{C_D S}{m} \tag{39}$$

Using the Space Shuttle value of q_{max} = 16,280 N/m^2 and plotting in the D-V plane yields the dynamic pressure constraint, as shown in Figure 20 (Harpold and Graves, 1978:103):

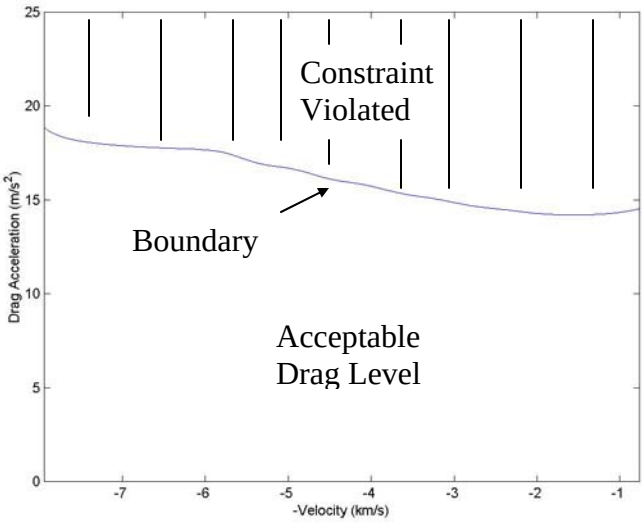

Figure 19: Normal Load Constraint in D-V Plane

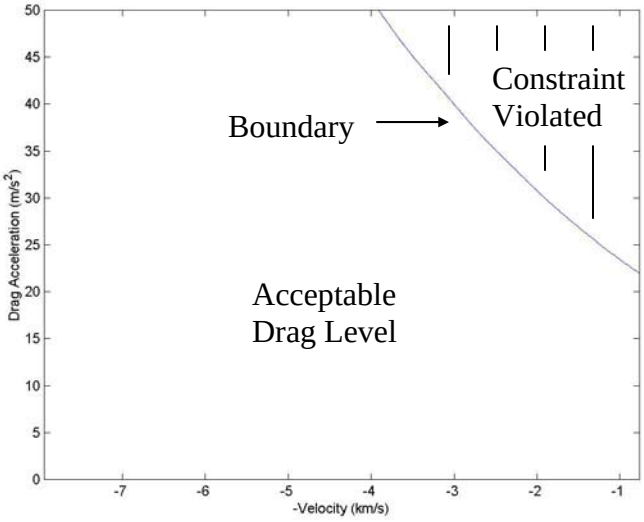

Figure 20: Dynamic Pressure Constraint in D-V Plane

Equilibrium Glide Constraint.

The final constraint to determine in the D-V plane is the equilibrium glide constraint. The equilibrium glide constraint is associated with the maximum range achievable. To determine the constraint, the flight path angle is held constant and the bank angle is set to 0, therefore achieving the minimum drag level (Lu, 1997:145). Then, from Equation (2) with the flight path angle assumed small, ie $\gamma \cong 0$:

$$\frac{L}{m} \geq \left(\frac{-V^2}{\mathrm{Re}+h} + g\right) \tag{40}$$

Substitute:

$$\frac{L}{m} = \frac{D}{m}\frac{L}{D} \tag{41}$$

and,

$$\frac{L}{D} = \frac{C_L}{C_D} \tag{42}$$

to get:

$$\frac{D}{m} \geq \frac{C_D}{C_L}\left(\frac{-V^2}{\mathrm{Re}+h} + g\right) \tag{43}$$

Plotting this equation in the D-V yields the equilibrium glide slope constraint as shown in Figure 21:

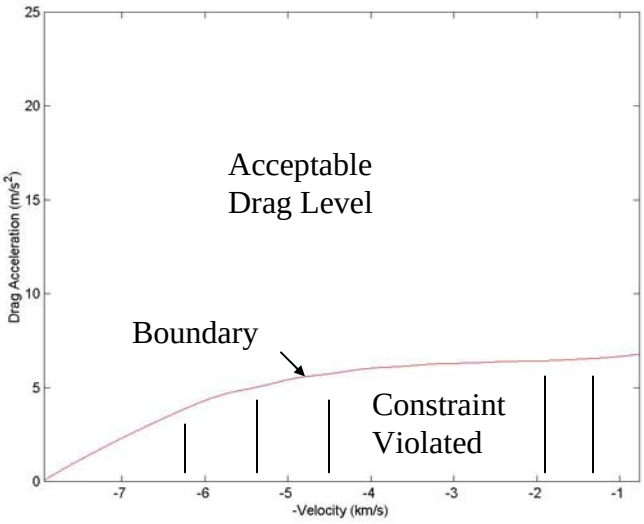

Figure 21: Equilibrium Glide Slope Constraint

Plotting all four constraints together defines the reentry corridor in the D-V plane as shown in Figure 22. An effective entry guidance controller will guide the vehicle's trajectory in such a way as to not violate any of the determined entry constraints, while at the same time controlling the vehicles energy such that the entry guidance termination point is reached at the desired energy state.

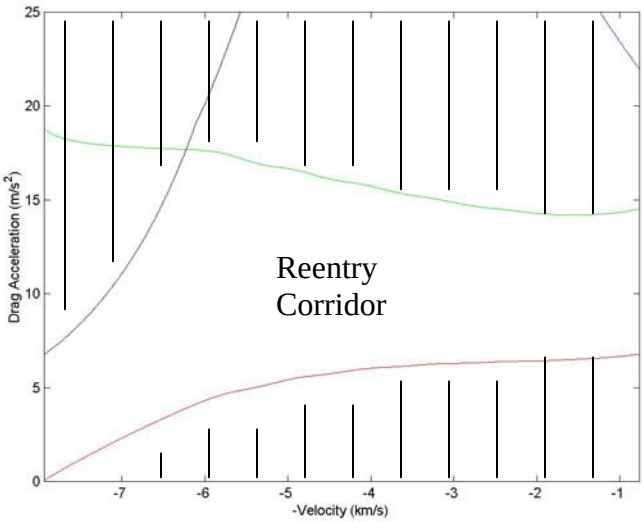

Figure 22: D-V Plane Reentry Corridor for SMV

Reference Profile

The previous section defined the reentry corridor in the D-V plane for the SMV. Next a reference profile that falls within the corridor will be developed. The reference profile will be constructed of three segments: the temperature control segment, the constant drag segment, and the transition segment (Harpold & Graves, 1978:109).

Temperature Control .

The primary concern during the early stages of atmospheric reentry is the heating rate constraint. The reference profile is developed by choosing a drag acceleration level at the initial velocity which lies within the reentry corridor. Next, a termination velocity is chosen for the temperature control segment. For the termination velocity, a drag

acceleration level within the reentry corridor is chosen. Then, drag acceleration at any point in the temperature control region is given by:

$$D = C_1 + C_2 V + C_3 V^2 \tag{44}$$

where the constant $C_3 = 3*10^{-4}$ km^{-1} and C_1 and C_2 are determined by the initial and final values of velocity and drag (Harpold & Graves, 1978:109).

Constant Drag.

The initial velocity and drag acceleration for the constant drag segment are the same as the termination velocity and drag acceleration for the temperature control region. Since the drag acceleration level remains constant throughout this region,

$$D = C_4 \tag{45}$$

defines the drag level (Harpold & Graves, 1978:109). Then, a termination velocity which, given the drag level, lies within the reentry corridor is chosen.

Transition.

The transition region controls the vehicle from its constant drag profile to the desired conditions at entry termination. The initial conditions for the transition region will be the same as the final conditions of the constant drag region. The termination conditions are dictated by the boundary conditions for entry guidance termination established earlier. Given those conditions, the following equation can be solved for C_5 and the drag acceleration level at any point in the region can be determined (Harpold & Graves, 1978:109):

$$D = D_F + C_5(E - E_F) \tag{46}$$

where:

D_F = drag acceleration level at entry guidance termination (km/s^2)

E_F = specific energy at entry guidance termination (km^2/s^2)

The reference profile can then be plotted in the D-V plane with the reentry corridor as shown in Figure 23:

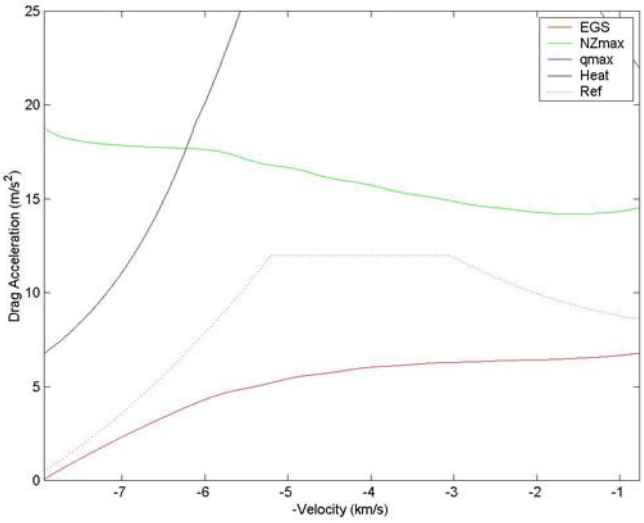

Figure 23: D-V Plane Reference Profile for SMV

Guidance

The guidance approach applied here is the approach used for Shuttle entry guidance. The guidance algorithm "is designed on the principal of analytically defining a desired drag acceleration profile and commanding the (vehicle) attitudes to achieve the desired profile" (Harpold and Graves, 1978:103). With the reference drag profile defined, it remains to determine a method to control the vehicle to this profile. The two

parameters available for controlling the vehicle to this profile are angle of attack, α, and bank angle, ϕ. Using bank angle as the primary trajectory control parameter allows the selection of an angle of attack profile which will provide desirable geometry for thermal protection (Harpold & Graves, 1978:105). Thus, the bank angle is modulated to control the vehicle to the reference drag profile. In doing this, the total entry range and crossrange are also controlled by the bank angle (Harpold & Graves, 1978:105). Then, angle of attack modulation is used for short period trajectory control, such as during a roll-reversal when the bank angle will roll through 0° and thus drive the vehicle to a lower than desired drag acceleration level.

Range Modulation.

The guidance algorithm is implemented at 1 sec intervals throughout the reentry trajectory. At each instance, the reference drag acceleration profile is updated to account for differences between nominal range to go and actual range to go. The nominal range to go is a summation of the nominal range to go in each of the three phases of reentry--temperature control, constant drag, and transition—and is calculated by (Harpold and Graves, 1978:109):

$$Q = 4C_3C_1 - C_2^{\,2}$$

$$if\ Q > 0$$

$$R_1 = \frac{-1}{2C_3}\ln[\frac{C_1 + C_2V_{F1} + C_3V_{F1}^{\,2}}{C_1 + C_2V\ + C_3V^{\,2}}]$$
$$+\frac{C_2}{C_3\sqrt{Q}}[\tan^{-1}[\frac{2C_3V_{F1} + C_2}{\sqrt{Q}}] - \tan^{-1}[\frac{2C_3V\ + C_2}{\sqrt{Q}}]]$$

$$if\ Q < 0$$

$$R_1 = \frac{-1}{2C_3}\ln[\frac{C_1 + C_2V_{F1} + C_3V_{F1}^{\,2}}{C_1 + C_2V\ + C_3V^{\,2}}]$$
$$+\frac{C_2}{2C_3\sqrt{-Q}}\ln\left[\frac{\frac{2C_3V_{F1} + C_2 - \sqrt{-Q}}{2C_3V_{F1} + C_2 + \sqrt{-Q}}}{\frac{2C_3V\ + C_2 - \sqrt{-Q}}{2C_3V\ + C_2 + \sqrt{-Q}}}\right] \quad (47)$$

where:

R_1 = Range to go in the temperature control region (km)

V = current vehicle velocity (km/s)

V_{F1} = velocity at termination of temperature control region (km/s)

Nominal range calculation in the constant drag region is done using (Harpold and Graves, 1978:109):

$$R_2 = \frac{V^2 - V_{F2}^{\,2}}{2C_4} \quad (48)$$

where:

V_{F2} = velocity at termination of constant drag region (km/s)

For the transition region, the nominal range to go is calculated by (Harpold and Graves, 1978:109):

$$R_3 = \frac{(E - E_{F3})}{(D - D_{F3})} \ln\left[\frac{D}{D_{F3}}\right] \tag{49}$$

where:

E_{F3} = specific energy at termination of entry guidance (km^2/s^2)

D_{F3} = drag acceleration level at termination of entry guidance (km/s^2)

During the first phase of reentry, only the temperature control reference drag acceleration profile is adjusted—the constant drag and transition reference profiles are not altered (Harpold and Graves, 1978:119). The effect of adjusting the reference profile in this manner is "to drive the trajectory back to nominal at the start of the constant drag phase" (Harpold and Graves, 1978:119). The same approach is taken during the constant drag phase where the transition reference drag profile remains unchanged.

Next, the actual range from the vehicle to the termination point is determined. The range, or rather the range angle, θ, can be determined using the current latitude and longitude of the vehicle and the latitude and longitude of the termination point, from (Pratt, 2003:34):

$$\cos\theta = \cos(L_v)\cos(L_F)\cos(l_v - l_f) + \sin(L_v)\sin(L_F) \tag{50}$$

where:

L_v = current latitude of vehicle

L_F = latitude of termination point

l_v = current longitude of vehicle

l_F = longitude of termination point

Then, the actual range to go is determined by:

$$R = \mathrm{Re}\,\theta \tag{51}$$

and the range error, ΔR,

$$\Delta R = R - R_N \tag{52}$$

where:

R_N = Nominal range to go (km) –determined by Equations (47-49)

In the temperature control phase of reentry, the constant C1 will be determined such that the updated drag reference profile meets range constraints. Then using the approximation for the derivative of range with respect to drag in the temperature control region (Tragesser 2003):

$$\frac{dR_1}{dD} = -\frac{R_1 + R_2}{(\frac{D_0 + D_{F1}}{2})} \tag{53}$$

Since,

$$\frac{dR_1}{dD} = \frac{dR_1}{dC_1}\frac{dC_1}{dD} = \frac{dC_1}{dD} \tag{54}$$

then, substituting and solving for dC_1:

$$dC_1 = -\frac{dR_1}{R_1}(\frac{D_0 + D_{F1}}{2}) \tag{55}$$

Then, for small time intervals,

$$\Delta R_1 = dR_1 \tag{56}$$

and R1 is calculated from Equation (47) above. Then, if ΔR is negative (nominal range is greater than actual range) the vehicle will be guided toward a higher reference drag profile since C_1 will be increased by dC_1.

As the reentry progresses the vehicle will transition from the temperature control phase to the constant drag phase. Once again, only the drag profile within this phase will be adjusted to null range errors. In the constant drag phase, the constant C_4 is modified to adjust the drag reference profile. The variation of range with C_4 is immediately apparent from:

$$\frac{dR_2}{dD} = \frac{dR_2}{dC_4}\frac{dC_4}{dD} = \frac{dR_2}{dC_4} \tag{57}$$

since $D=C_4$. Then, with $dR_2 = \Delta R$, differentiating Equation (48) and solving for dC_4 gives (Tragesser 2003):

$$dC_4 = \frac{-2C_4{}^2 dR_2}{V^2 - V_{F2}{}^2} \tag{58}$$

As in the temperature control region if ΔR is negative, dC_4 will be positive, causing the vehicle to be guided toward a higher drag profile.

For the transition phase of reentry, the constant C_5 will be modified to null range errors. The derivative of range with respect to C_5 can be determined by first rearranging the drag equation for the transition phase (Equation 46) and solving for C_5:

$$C_5 = \frac{(D - D_{F3})}{(E - E_{F3})} \tag{59}$$

and substituting into Equation (49):

$$R_3 = \frac{1}{C_5} \ln\left[\frac{D}{D_{F3}}\right] \tag{60}$$

Then, taking the derivative with respect to C_5 yields (Tragesser 2003):

$$dC_5 = \frac{dR_3}{\frac{1}{C_5}\left[-R_3 + \frac{E - E_{F3}}{D}\right]} \tag{61}$$

Once again, with $dR_3 = \Delta R$, C5 will be increased, and therefore the drag profile increased when the nominal range exceeds the actual range.

Bank Angle Modulation.

The previous section determined the variance of C_1, C_4, and C_5 to account for range errors. This section will show how these updated coefficients are used to determine the appropriate angle of attack to guide the vehicle to the reference drag acceleration profile.

Once the updated drag acceleration profile is defined, the desired L/D and altitude rate corresponding to the drag acceleration profile need to be determined (Harpold and Graves, 1978:109). These parameters are then used in the control law to command the vehicle to the reference profile (Harpold and Graves, 1978:109). The equations for L/D and altitude rate are presented in *Shuttle Entry Guidance* and listed in Table 4, with the approximation that $\dot{C}_D = \ddot{C}_D = 0$ (Harpold and Graves, 1978:109). Using these equations, a "control law based on linearized analysis of the flight dynamics, which ensures damping of oscillatory type trajectory motion" can be implemented (Harpold and Graves, 1978:113).

Table 4: Reference Trajectory Parameters

Phase	D_0	$\dot{h}_0$	$(L/D)_0$
Temperature Control	$C_1 + C_2V + C_3V^2$	$\frac{-H}{V}[2C_1 + C_2V]$	$\frac{g}{D_0}\left[1-\frac{V^2}{V_s^2}\right]-\frac{4HC_1}{V^2}-\frac{HC_2}{V}$
Constant Drag	C_4	$-H\left[\frac{2D_0}{V}\right]$	$\frac{g}{D_0}\left[1-\frac{V^2}{V_s^2}\right]-\frac{4HD_0}{V^2}$
Transition Phase	$D_F + C_5(E-E_F)$	$-H\left[\frac{2D_0V-C_5V^3}{V^2+2Hg}\right]$	$\frac{g}{D_0}\left[1-\frac{V^2}{V_s^2}\right]+\frac{1}{V^2+2gH}$ *$(2V\dot{h}_0+\frac{2\dot{h}_0^2 g}{D}-C_5HV^2$ $+2D_0H+2g\dot{h}_0\frac{H}{V}$ $-3C_5Vg\dot{h}_0\frac{H}{D_0})+\frac{\dot{h}_0}{V}+\frac{g\dot{h}_0^2}{D_0V^2}$

The resulting control law, with f_4=0 is (Harpold and Graves, 1978:113):

$$(\frac{L}{D})_c = (\frac{L}{D})_0 + f_1(D-D_0) + f_2(\dot{h}-\dot{h}_0) \tag{62}$$

where:

$(\frac{L}{D})_c$ = commanded L/D

The theoretical gains (f_1 and f_2) in the control law are complex and lengthy equations, and therefore, are not used in the flight software (Harpold and Graves, 1978:123). Instead, the following empirical curve fits as functions of drag are used to determine the gains:

$$f_1 = f_5 D^{f_6} + f_9 (D - D_0)$$
$$f_2 = f_7 D^{f_8} \tag{63}$$

where the coefficients "f_5, f_6, f_7, f_8, and f_9 are empirically derived constants used to fit the f_1 and f_2 theoretical functions" (Harpold and Graves, 1978:123). In this study, the curves used for f_1 and f_2 for Shuttle entry guidance were used to determine the empirical coefficients. In the case of the controller gain, f_2, the values used herein are the negatives of those provided in Harpold and Graves—this is attributable to the definition of positive flight path angle below the horizontal (1978:124). Figures 24 and 25 show the controller gains as functions of drag.

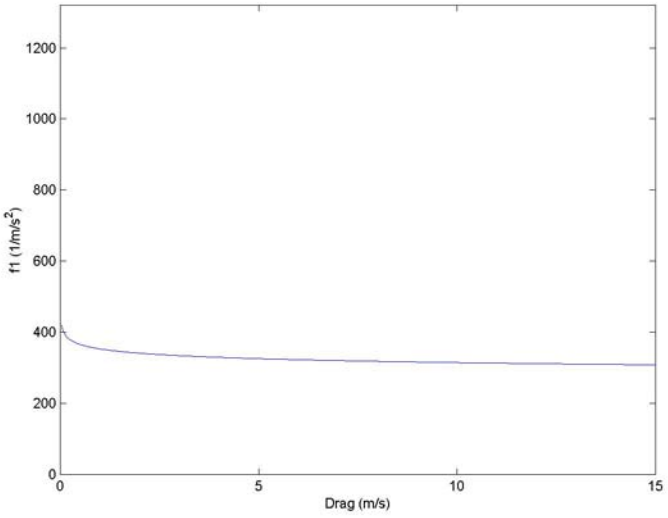

Figure 24: Controller Gain (f_1)

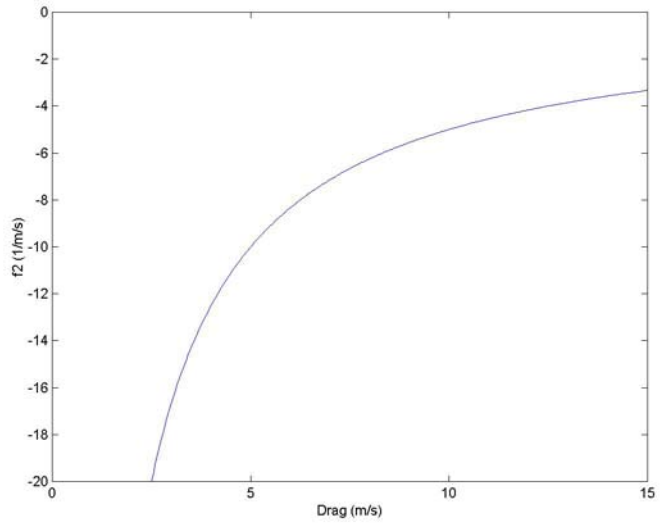

Figure 25: Controller Gain (f_2)

The $(L/D)_c$ determined from the control law is then used to determine the bank angle from (Harpold and Graves, 1978:124):

$$\phi_C = \cos^{-1}\left[\frac{(L/D)_c}{(L/D)}\right] + f_{11}(\alpha - \alpha_0) \tag{64}$$

where:

ϕ_c = commanded angle of attack

L/D = current lift-to-drag ratio

f_{11} = controller gain

α = current angle of attack

α_0 = reference angle of attack

In addition, angle of attack modulation is used for short period drag control, such as is required during a roll reversal (Harpold and Graves, 1978:125). Angle of attack modulation is controlled by (Harpold and Graves, 1978:125):

$$\Delta\alpha = \alpha - \alpha_0 = C_D(D_0 - D) / f_{10} \tag{65}$$

where f_{10} is a controller gain. During a roll reversal, the angle of attack will be increased, thus creating higher drag. The last term in Equation (65) acts to drive the angle of attack back to the nominal profile (Harpold and Graves, 1978:125).

The control algorithm developed above is implemented subjected to a roll constraint. The constraint is to limit the bank angle rate to 5 degrees per second. Thus, each time the control algorithm is implemented, a commanded bank angle is determined. This commanded bank angle is then compared to the current bank angle to see if it is achievable within the prescribed constraint of 5°/s roll rate.

Roll Reversal.

As the vehicle reenters the atmosphere, the bank angle will be modulated to control to the reference drag profile and to null range errors. In order to reach the desired termination point, the vehicle will have to reverse the direction of bank at certain points along the trajectory. The prior discussions addressed how the drag acceleration was affected by the roll reversal. The discussion here will focus on when roll reversals are implemented. It is desirable to maintain a heading angle which is within some given deadband of the desired heading angle. Desired heading angle is calculated as the heading angle at which the vehicle would travel from its current location to the

termination point along a great circle route. This angle, desired azimuth, AZ_D, is calculated from:

$$AZ_D = \tan^{-1} \frac{\cos(L_F)\sin(l_F - l_v)}{\cos(L_v)\sin(L_F) - \sin(L_v)\cos(L_F)\cos(l_F - l_v)} \tag{66}$$

The deadband used for heading angle control is as shown in figure 26:

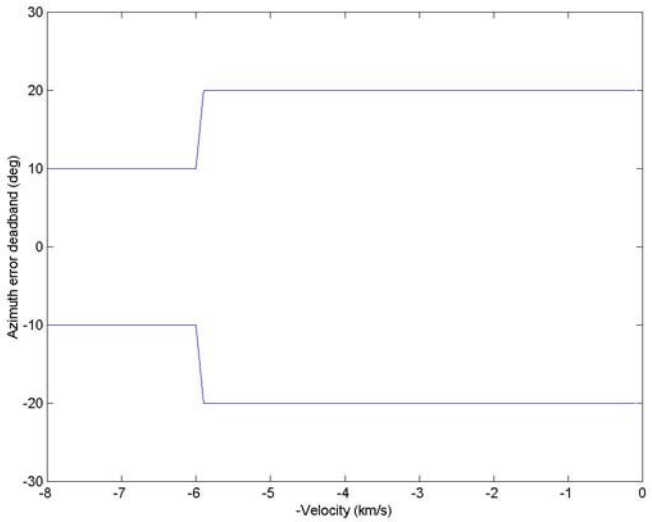

Figure 26: Azimuth Error Deadband

The actual heading angle of the vehicle is calculated from Equation (3) and compared with the deadband. When the deadband is exceeded a roll reversal will be commanded.

IV. Results

Chapter Overview

This chapter will present the results obtained when applying the drag profile guidance concept to the developed SMV model. Two mission profiles will be examined and an error analysis will be conducted.

High-Inclination Orbit

The first case considered will be a 75°-inclination orbit with no crossrange requirement. The initial orbit altitude is 500 km. A deorbit burn of 121 m/s (397 ft/s) will put the vehicle on a Hohmann transfer ellipse to an altitude of 80 km, with reentry beginning at 122.2 km. The initial velocity is 7.94 km/s and the initial flight path angle at 122.2 km is 1.09°. The landing site is at Kennedy Space Center, FL.

Figure 27 shows the ground trace of the initial 75° orbit, along with the location at which reentry begins at 122.2 km, and the landing site.

Figure 28 is a plot of altitude versus distance for the reentry. During the initial stages of reentry, approximately 2000 km of range, the plot is essentially linear as the flight path angle, γ, is essentially constant. At approximately 80 km the effects of the sensible atmosphere begin to slow the vehicle's descent.

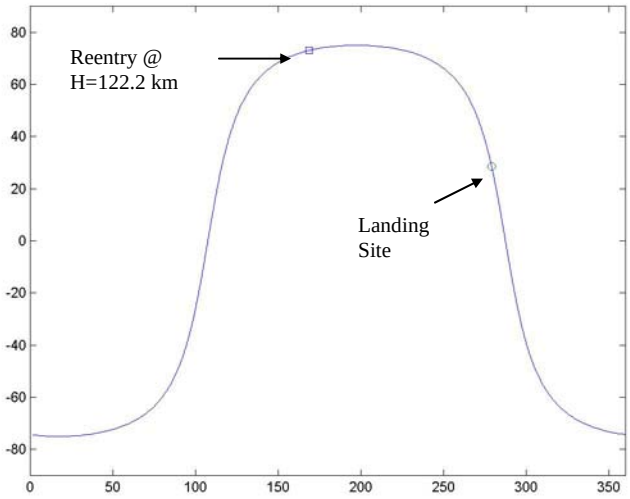

Figure 27: Ground Trace of Orbit (i=75°)

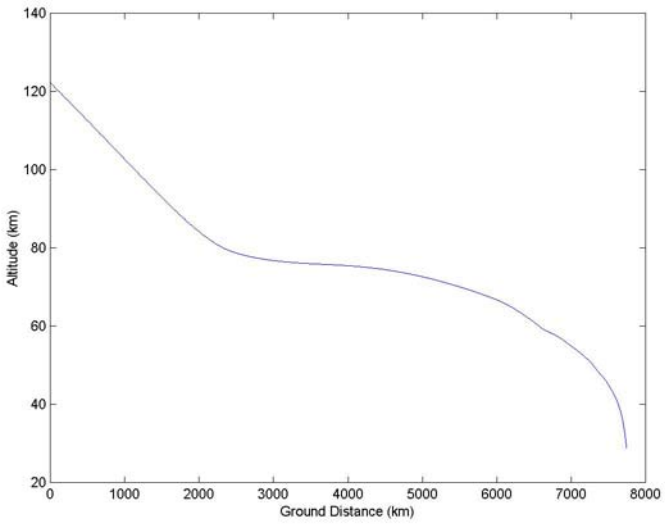

Figure 28: Altitude vs. Range (i=75°)

The increased atmospheric effects at about 80 km altitude can also be seen in Figure 29, which shows the variation of velocity with respect to altitude. The velocity remains

nearly constant over 40 km of altitude. Once an altitude of approximately 80 km is reached, the velocity begins decreasing in a near-linear manner.

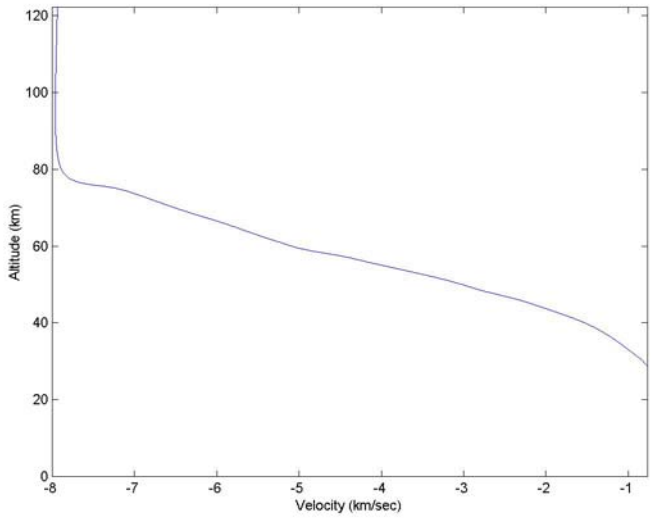

Figure 29: Altitude vs. Velocity (i=75°)

Figure 30 shows the reentry corridor, the reference profile, and the actual trajectory in the D-V plane.

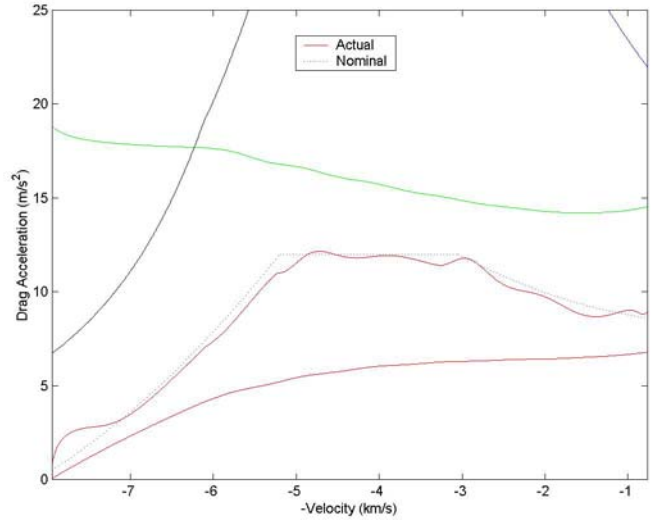

Figure 30: SMV Reentry Profile in D-V Plane (i=75°)

During the initial stages of reentry the heating constraint is the primary concern. In particular, the region of concern is from an altitude of approximately 85 km down to an altitude of 75 km—this corresponds with the region at the beginning of the corridor where the actual drag acceleration level is significantly higher than the nominal drag acceleration level. At approximately 6 km/s, which corresponds to an altitude of 65 km, the maximum normal load becomes the limiting constraint.

The variation of the bank angle with respect to velocity is shown in Figure 31.

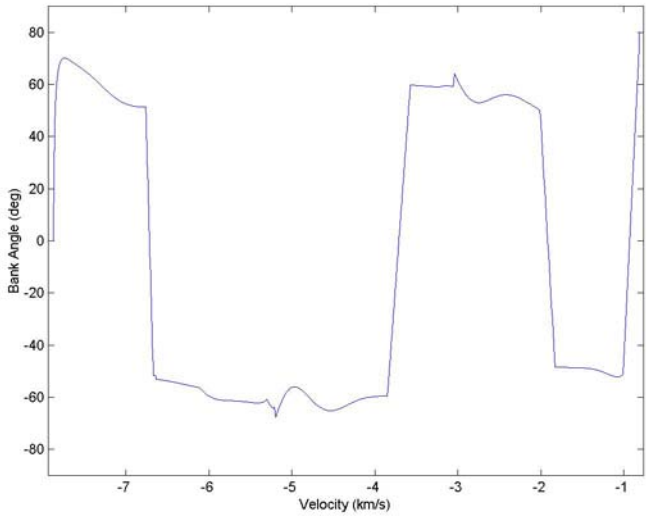

Figure 31: Bank Angle vs. Velocity (i=75°)

The bank angle, ϕ, is modulated to control the drag acceleration level and to null range errors. The modulation is fairly smooth except in the regions where the guidance shifts from one phase to the next. At these transition points, peaks are seen in the bank angle history as the vehicle attempts to reach nominal conditions before entering the next phase. The bank angle history shows that the vehicle will perform 4 roll reversals in order to stay on azimuth for the termination point.

Figure 32 shows the angle of attack modulation throughout the reentry, compared with the nominal angle of attack profile. The commanded angle of attack agrees closely with the reference angle of attack profile, since the bank angle is being modulated to control drag acceleration levels and null range errors.

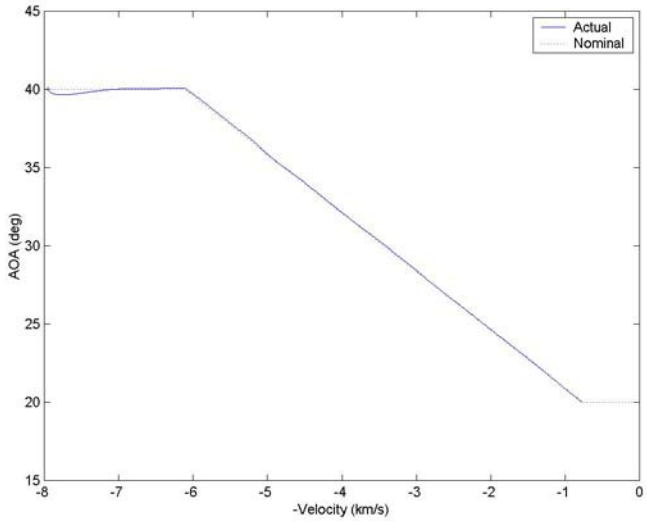

Figure 32: Angle of Attack vs. Velocity (i=75°)

Figure 33 is a plot of the actual and desired azimuth angle during reentry. The actual azimuth angle drifts within the deadband through the reentry. Whenever the deadband is exceeded, a roll reversal is commanded (as shown in Figure 31).

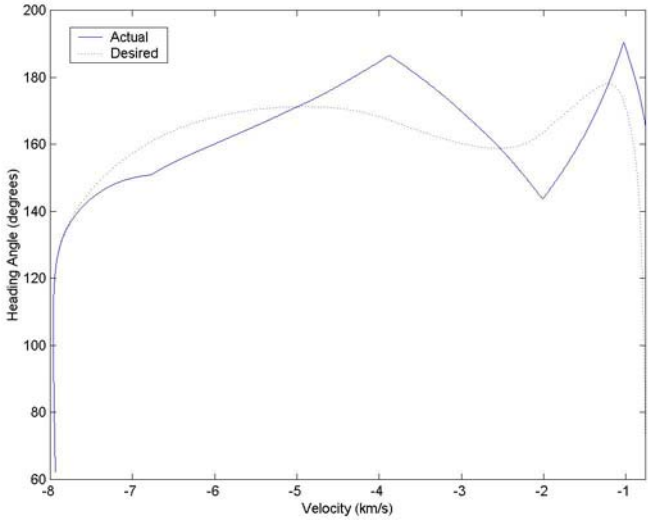

Figure 33: Azimuth angle vs. Velocity (i=75°)

Figure 34 is a plot of the flight path angle, γ, versus velocity. The flight path angle is 1.09° at initial reentry and decreases to a minimum of 0.06° at an altitude of 76 km. For the majority of the reentry, the flight path angle remains between 0° and 2°. As

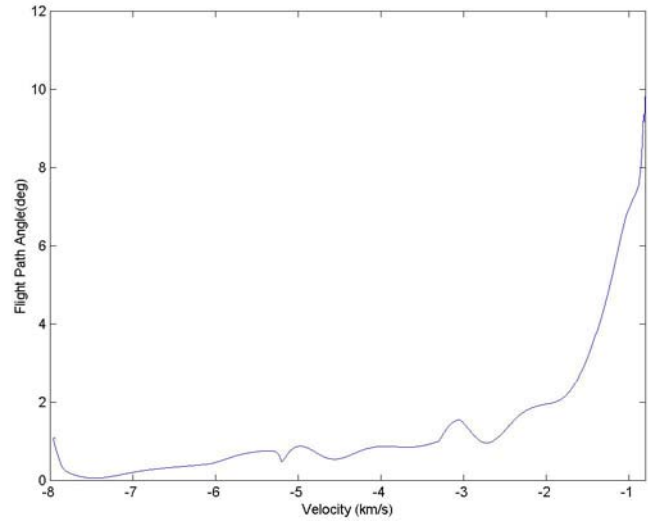

Figure 34: Flight Path Angle vs. Velocity (i=75°)

the velocity decreases below 2 km/s the flight path angle begins decreasing rapidly, and the vehicle's rate of descent increases.

The primary goal of the guidance algorithm employed in this study is to guide the vehicle through the established reentry corridor to a termination point at an acceptable energy state for approach and landing. Figure 30 shows the successful guidance through the reentry corridor without violation of constraints. As for the acceptable energy state at the termination point, Table 5 presents a comparison of the actual and nominal terminal values for velocity, altitude, and position for this scenario. Figure 35 shows the ground trace of the reentry profile.

Table 5: Terminal Conditions for SMV Reentry (i=75°)

Conditions	**Nominal**	**Actual**	**Guidance Error**
Velocity	0.764 km/s	0.764 km/s	0 km/s
Altitude	29.4 km	28.8 km	-.6 km
Latitude	28.60° N	28.59° N	-.01°
Longitude	279.10° E	279.05° E	-.05°

Thus, the vehicle was accurately guided to within 3.8 km of the termination point at an altitude of –0.6 km below the nominal desired altitude, without violating reentry constraints.

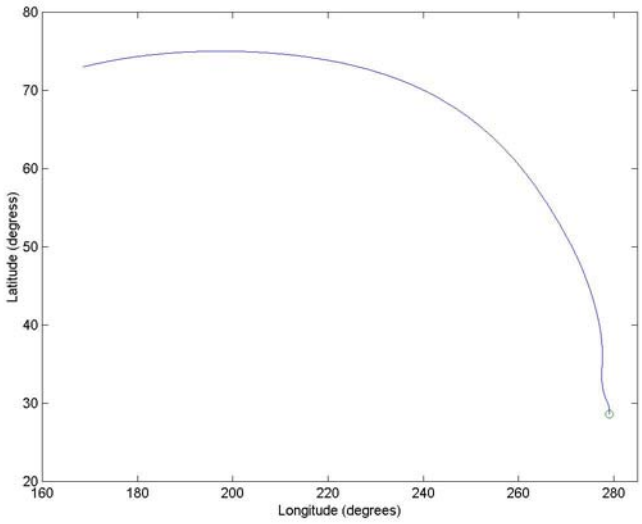

Figure 35: Ground Track of SMV Reentry Path (i=75°)

Low Inclination Orbit with Cross Range Requirement

The second case will look at the reentry profile for a vehicle in an orbital plane which does not pass directly over the terminal point. The initial altitude will again be 500km, thus the deorbit burn, initial velocity, and initial flight path angle will be the same as calculated in the first case:

$$\Delta V = 121 \text{ m/s} = 397 \text{ fps}$$

$$V_0 = 7.94 \text{ km/s} = 26000 \text{ ft/s}$$

$$\gamma_0 = 1.09°$$

The inclination will be 28.6°. For this scenario, a hypothetical orbit at 28.6° inclination which passes directly overhead of the terminal point will be referred to as the nominal orbit. The actual initial orbit of the vehicle will be rotated 22.5° to the West from the nominal. That is, the right ascension of the ascending node of the actual orbit will be

22.5° West of the right ascension of the ascending node of the nominal orbit. The setup is depicted in Figure 36. This scenario is significant in that, for a rotating earth, it represents the single orbit (or Abort Once Around) scenario.

Figure 37 shows that the variation of altitude with respect to range is similar to the high-inclination scenario.

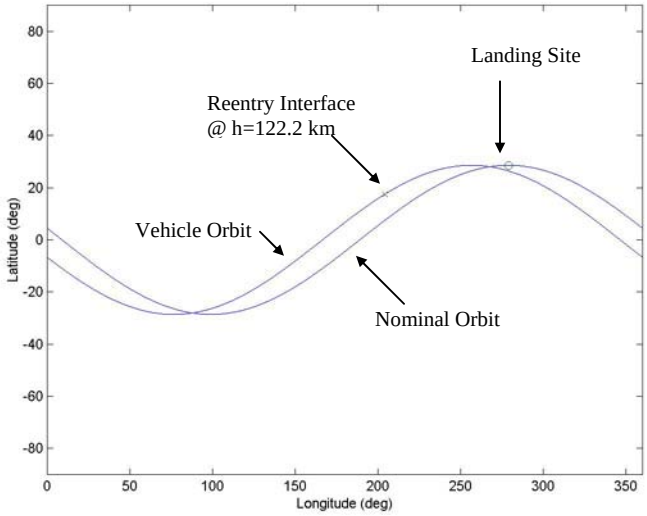

Figure 36: Ground Trace of Actual and Nominal Orbits (i=28.6°)

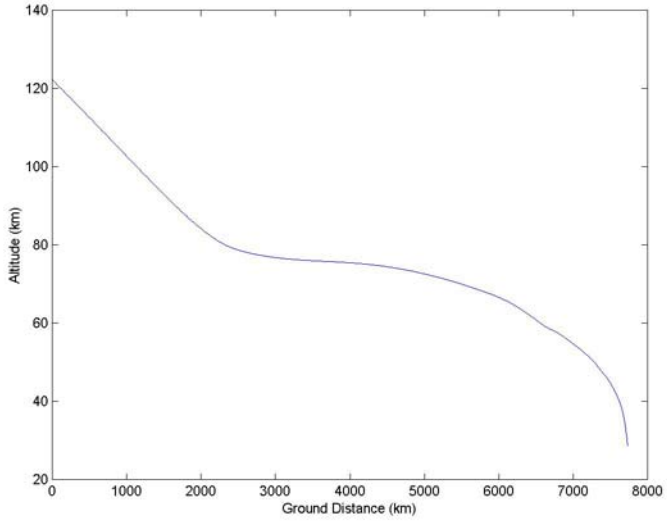

Figure 37: Altitude vs. Range (i=28.6°)

In Figure 38 it can be seen that once again the velocity remains essentially constant until an altitude of approximately 80km.

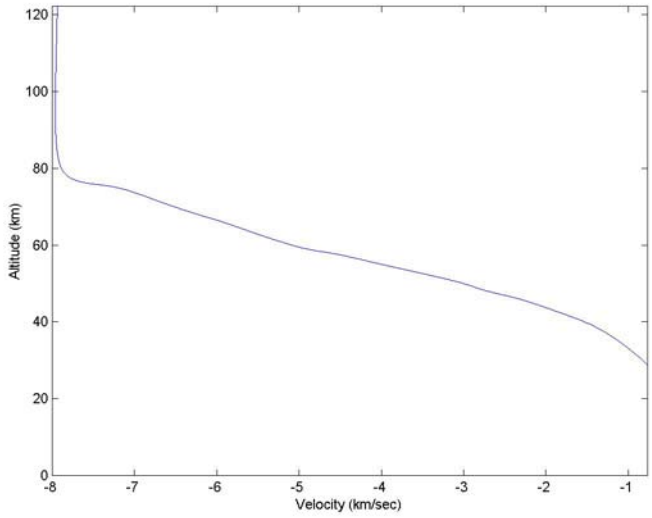

Figure 38: Altitude vs. Velocity (i=28.6°)

Figure 39 shows the vehicle's reentry profile in the D-V plane. Once again, there is a period of increased drag early in the profile, but the heating constraint is not violated.

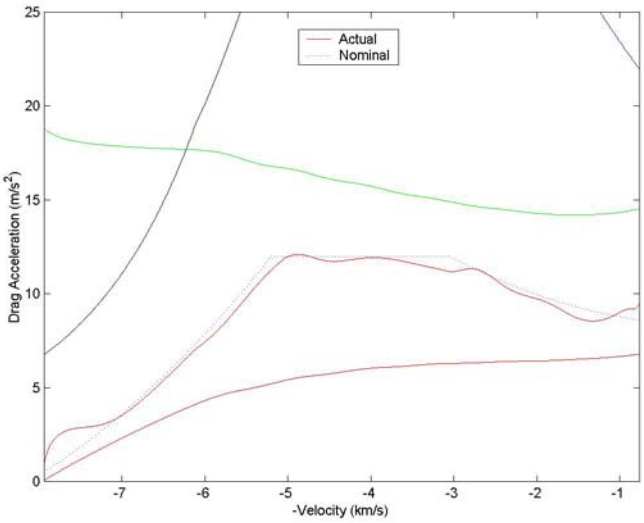

Figure 39: SMV Reentry Profile in D-V Plane (i=28.6°)

Figure 40 shows the bank angle modulation for this reentry profile. Since the landing site does not lie in the plane of the orbit, the initial azimuth and the desired azimuth are not the same—as shown in Figure 41.

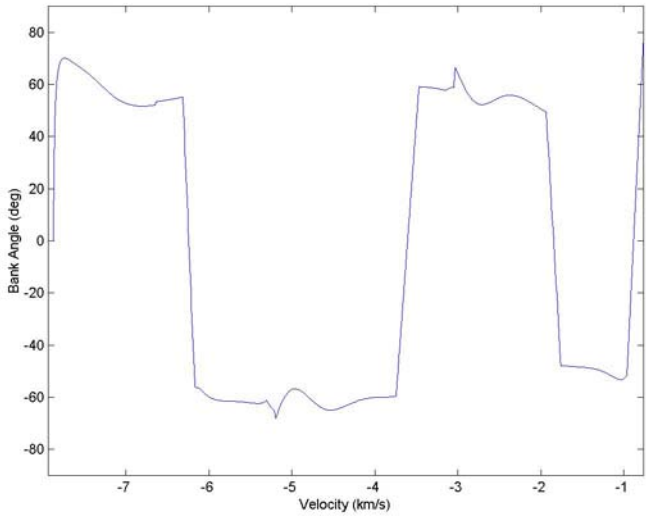

Figure 40: Bank Angle vs. Velocity (i=28.6°)

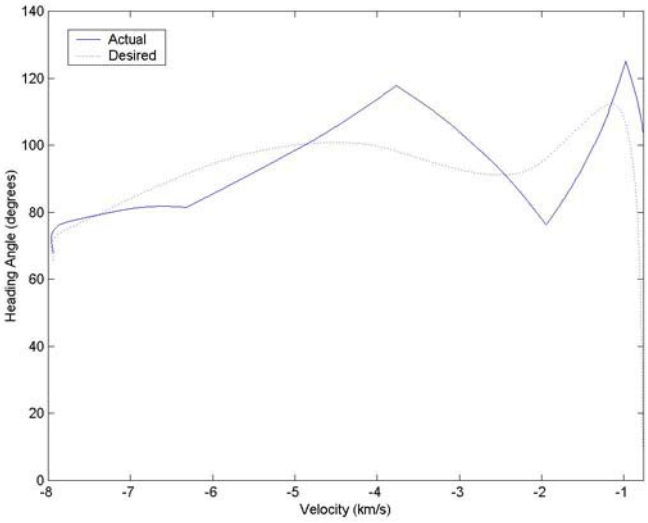

Figure 41: Azimuth angle vs. Velocity (i=28.6°)

Figure 42 depicts the actual and nominal angle of attack profiles for this scenario, and Figure 43 shows the flight path angle as a function of velocity.

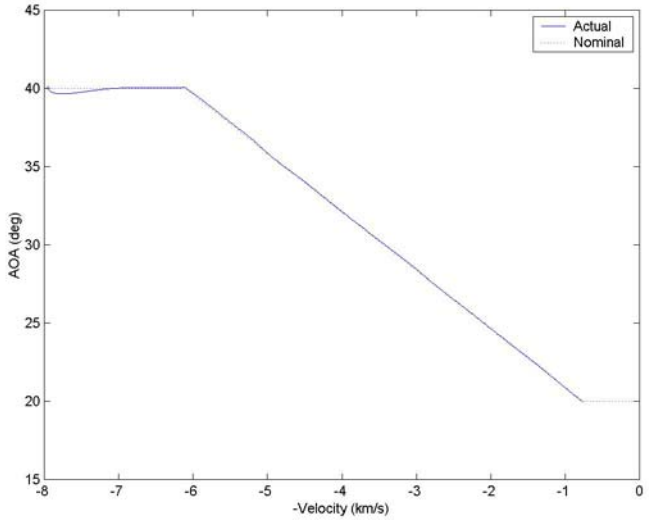

Figure 42: Angle of Attack vs. Velocity (i=28.6°)

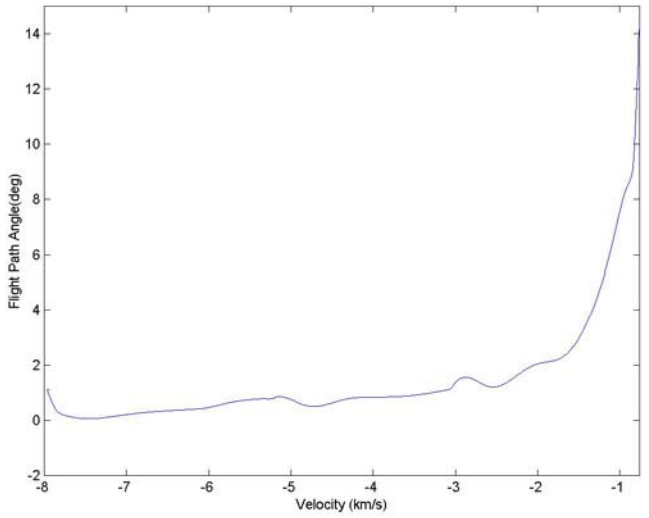

Figure 43: Flight Path Angle vs. Velocity (i=28.6°)

The nominal terminal conditions for the energy state and position at entry guidance termination are the same as calculated previously. Figure 44 shows the ground track of the reentry profile, and Table 6 summarizes the final conditions.

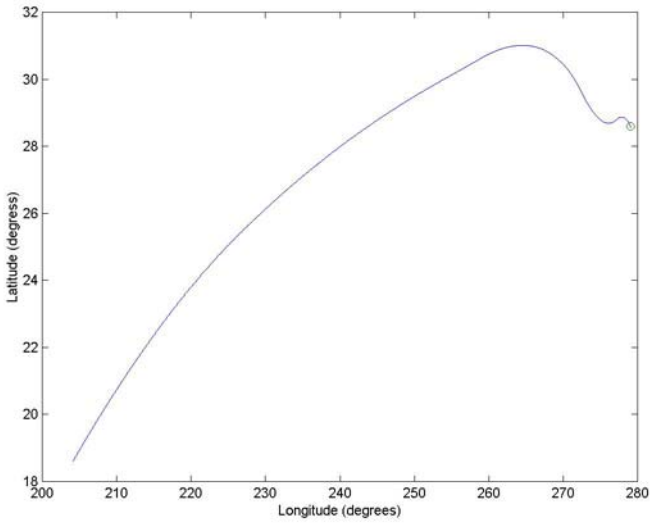

Figure 44: Ground Track of SMV Reentry Path (i=28.6°)

Table 6: Terminal Conditions for SMV Reentry (i=28.6°)

Conditions	Nominal	Actual	Guidance Error
Velocity	0.764 km/s	0.765 km/s	+.001 km/s
Altitude	29.4 km	28.7 km	-.7 km
Latitude	28.60° N	28.56° N	-.04°
Longitude	279.10° E	279.09° E	-.01°

The final position corresponds to a 4.02 km position error at entry guidance termination.

Error Analysis

In order to complete the analysis of the application of the developed guidance algorithm to the SMV, it is appropriate to perform an error analysis. Errors in the initial

state of the vehicle will cause the profile to be shifted off the nominal profile. A functional guidance system should be capable of guiding the vehicle to the termination point, without violating entry constraints, in the presence of errors. Possible sources of error for the vehicle initial state include: altitude at guidance initiation, variations in initial orbital parameters, and thruster (deorbit ΔV) inaccuracies. In addition to errors in the initial state, variations in the aerodynamic properties (C_L and C_D) as well as atmospheric variations should be considered.

For the purposes of error analysis in this study, a Monte Carlo analysis will be conducted. "For a given Monte Carlo trajectory the Gaussian random number generator is entered with the appropriate standard deviation, the output is added algebraically to the mean value and the trajectory is run" (Regan, 1993:449).

High Inclination Orbit Error Analysis.

For this analysis, the profile as setup in scenario 1 above will be used—high inclination orbit with no crossrange requirement. The mean values for use in the Monte Carlo simulation will be the nominal value for each initial condition, as previously calculated. The standard deviation will then be used to estimate the magnitude of the error for each condition. Table 7 summarizes the parameters to be used in the error analysis.

Table 7: Initial Conditions and Uncertainties for Monte Carlo Analysis

Initial Conditions	Mean Value	Standard Deviation
Velocity	7.94 km/s	.01 km/s
Flight Path Angle	1.09°	.01°
Azimuth Angle	62.24°	0.1°
Altitude	122.2 km	1 km
Latitude	73.01° N	0.5°
Longitude	168.65° W	0.5°

For the aerodynamic coefficients, the mean value is taken to be the value determined from the curve fits in Chapter 2 at the given angle of attack, and the standard deviation is taken to be 0.01. For atmospheric variations, the standard sea-level density is taken as the mean, and the standard deviation around the mean is 0.07 kg/m^3 (Regan 1993:449).

Figures 45 and 46 show the results of a 100-run Monte Carlo simulation for bank angle and angle of attack. Figure 47 shows the reentry corridor in the D-V plane along with the profiles followed for the 100 runs. Some variation is noted, especially near the transition points from one guidance phase to another, but the reentry constraints are not violated. Figure 48 is a plot of the termination points for the each run. The mean distance to the desired termination point at entry guidance termination is 3.82 km, with a standard deviation of 1.46 km. The maximum distance from the desired termination point is 10.79 km.

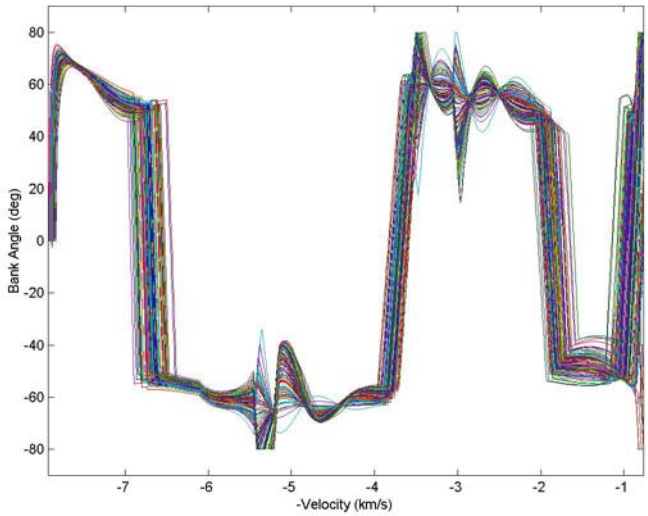

Figure 45: Bank Angle vs. Velocity for 100-Run Simulation

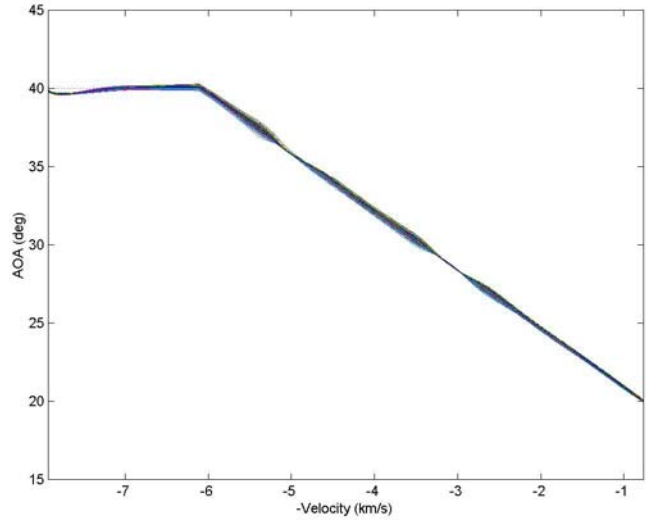

Figure 46: Angle of Attack vs. Velocity for 100-Run Simulation

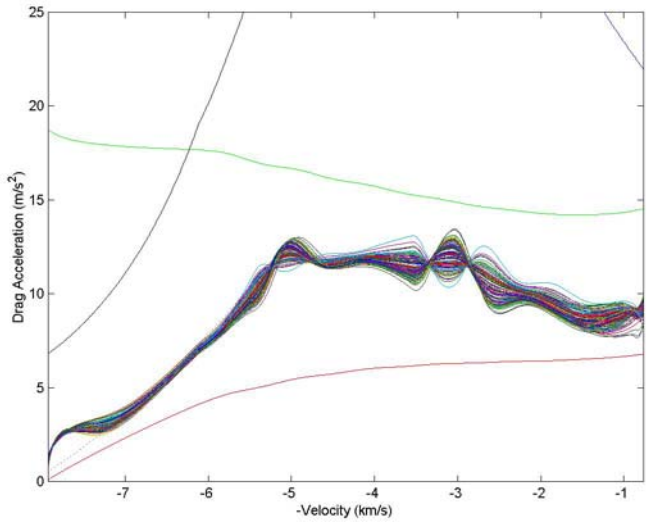

Figure 47: D-V Plane Reentry Profile for 100-Run Simulation

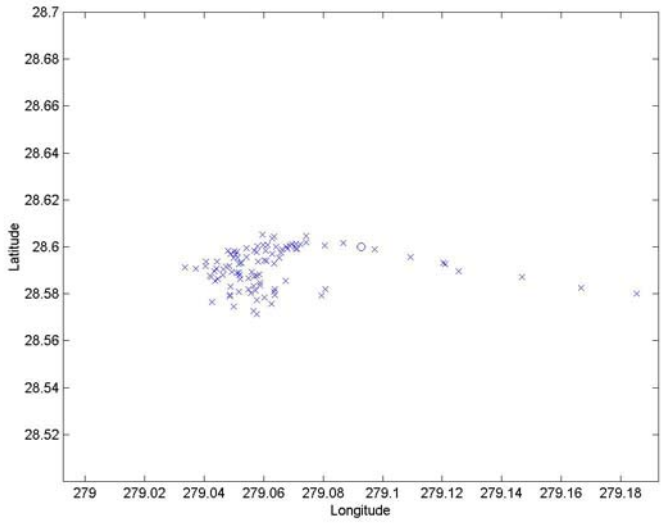

Figure 48: Entry Guidance Termination Location for 100-Run Simulation

The distribution of the altitude at termination is shown in Figure 49 with the mean altitude at entry guidance termination being 28.98 km and a standard deviation of 0.32 km.

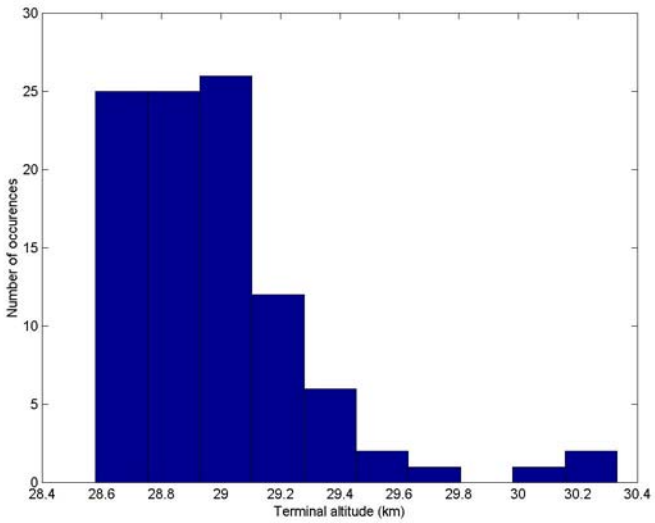

Figure 49: Altitude at Entry Guidance Termination for 100-Run Simulation

V. Conclusions and Recommendations

Results and Recommendations

The objective of this study was to determine a means of guiding a conceptual Space Maneuver Vehicle (SMV) through atmospheric reentry to a pre-determined entry guidance termination point. The strategy adopted to solve this problem was to apply the concepts used for Space Shuttle Orbiter reentry guidance to the SMV. Having done this, the following conclusions can be drawn from the results provided in Chapter 4.

1. The concept of selecting a desired drag acceleration profile and controlling the vehicle to that profile through bank angle modulation is an effective method for guiding the SMV for atmospheric reentry. The results for the two scenarios, as well as the 100-run Monte Carlo analysis, show that in all cases the vehicle is guided to the termination point, within the constraint corridor. In all cases, the energy state at guidance termination compares favorably with the desired energy state.

2. Although the entry initiation altitude was chosen to be 122.2 km, atmospheric effects are essentially negligible until the vehicle reaches an altitude near 80 km. Until 80 km altitude, the velocity and flight path angle remain essentially constant.

3. The control algorithm, as developed, shows some weakness in the region near the transition points from one guidance phase to the next. The discontinuities at the transition points in the nominal drag acceleration profile cause the controller to over-compensate in an effort to match range and drag acceleration levels at these points. As a result, "spikes" in the bank angle and drag acceleration profile occur.

4. The entry guidance algorithm developed is designed to accommodate prograde orbits from 0°-89.99° inclination. Retrograde orbits were not studied, however, minor modification to the algorithm should account for this type of orbit.

The following recommendations for further study are given:

1. The analysis conducted herein is somewhat limited by the assumptions made. Whereas this analysis could be used as an effective baseline, the fidelity of the simulation would have to be improved for an operational guidance method. In particular, a more robust model of the Earth's atmosphere accounting for cross-winds, hemispheric variations, and seasonal variations should be input into the guidance algorithm. Also, a higher order model of the Earth's gravitational field, to include variation with altitude, as well as oblateness effects should be incorporated.

2. The vehicle parameters used herein are all estimates for the Space Maneuver Vehicle. As the vehicle moves from the drawing board to the prototype phase, these parameters

will become more obtainable. The parameters of mass, wingspan, and area may not be affected, but the aerodynamics are likely to require modification. Construction of a higher-fidelity model than the one used herein for use in determining the aerodynamic coefficients is one possible approach. Ideally, as a prototype is developed, wind tunnel data and actual flight test data could be used to more accurately describe these coefficients in the entry guidance algorithm.

3. The concept of controlling the vehicle to a desired drag level used for Shuttle entry guidance is a tried and tested concept. A similar approach is to "define the reference profile as a function of the energy, specifically, a piecewise-linear, continuous function of the energy" (Lu, 1997:143). Using this approach preserves the analytical range prediction and allows for non-computationally intensive on-board determination of the optimal reference drag profile (Lu, 1997:143). As a course of further study, this concept could be applied to the SMV reentry guidance and compared with the results obtained using the D-V plane entry corridor.

4. Once again, the goal of this study was to develop an entry guidance controller for the SMV—not to optimize the reentry profile. The controller developed here could be used to determine optimal reentry trajectories in a further study. Studies of interest would include the determination of optimal profile for accumulated heat load or the determination of angle of attack profile to provide maximum crossrange.

Appendix A

Measurements are scaled to the vehicle length: L = 29 ft (8.84m)

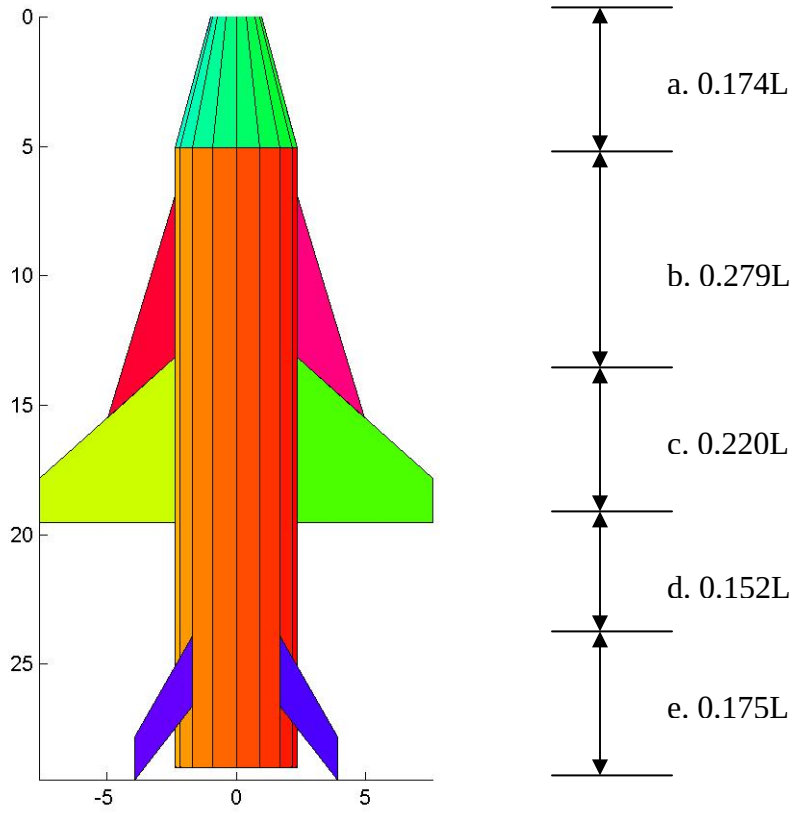

Figure 50: MATLAB SMV Model Top View 1

a. Nose Length
b. Length from Nose to forward lifting surface
c. Forward lifting surface inboard length
d. Length from rear of forward lifting surface to front of rear stabilizer
e. Length from front of rear stabilizer to rear of vehicle

Measurements are scaled to the vehicle length: L = 29 ft (8.84m)

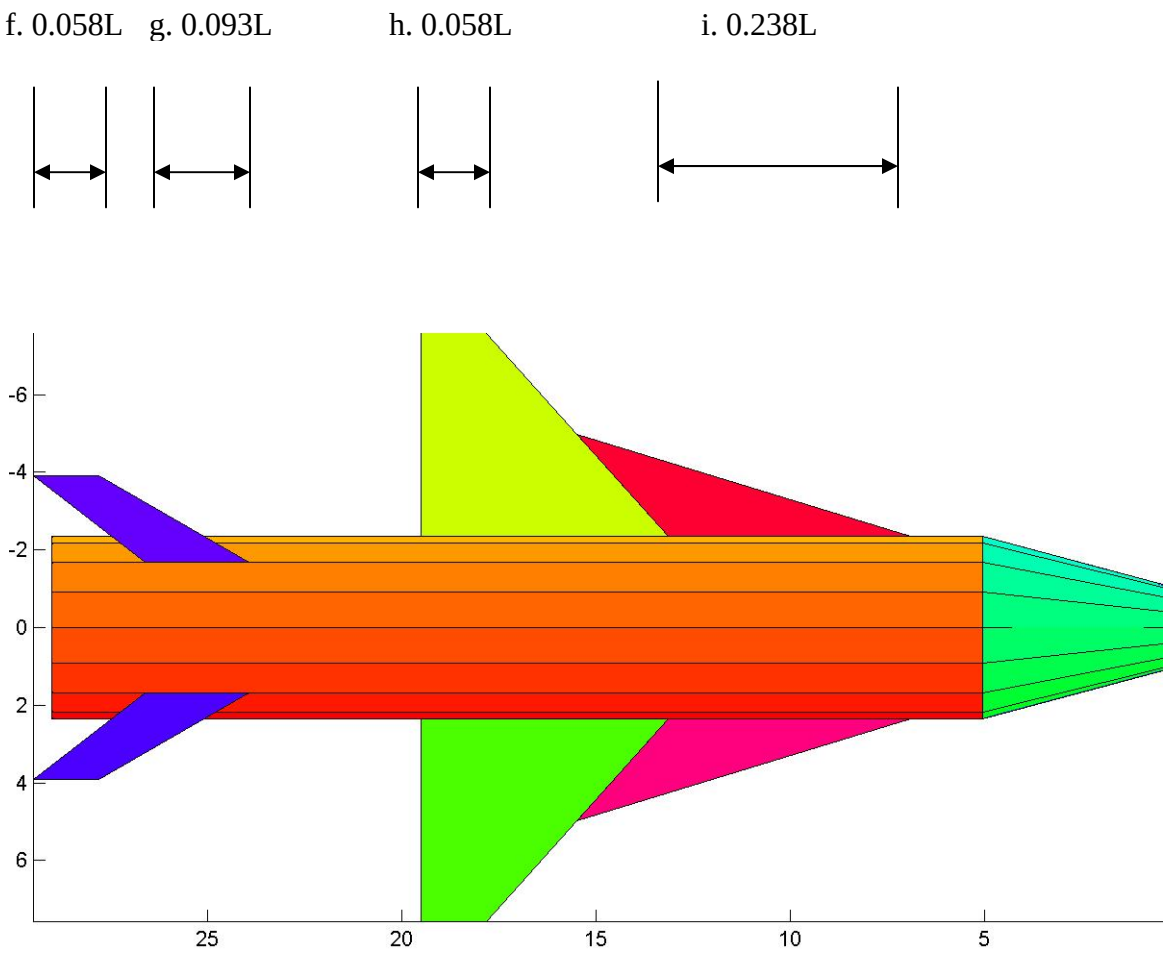

Figure 51: MATLAB SMV Model Top View 2

f. Rear stabilizer outboard length
g. Rear stabilizer inboard length
h. Forward lifting surface outboard length
i. Delta wing inboard length

Measurements are scaled to the vehicle length: L = 29 ft (8.84m)

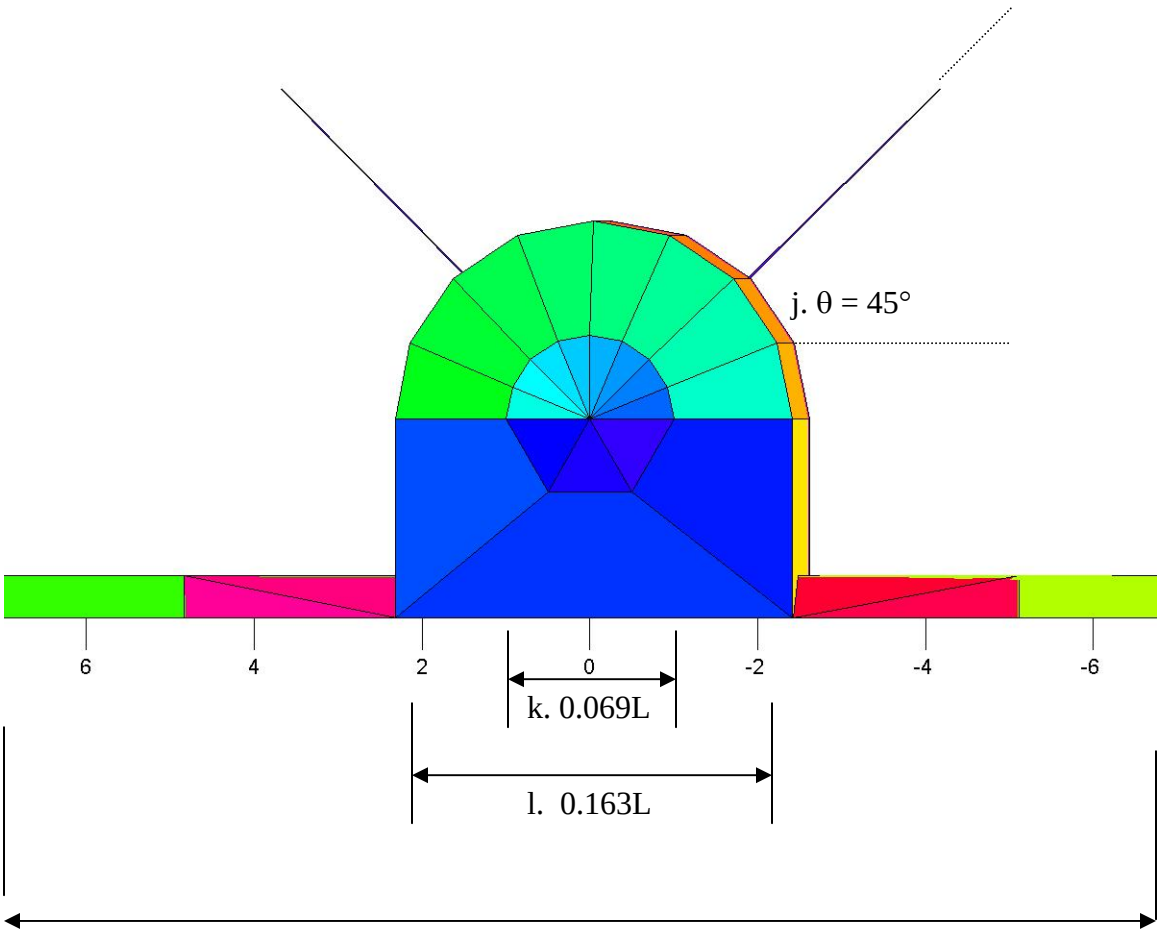

Figure 52: MATLAB SMV Model Front View

j. Rotation angle for Rear Stabilizer
k. Nose diameter
l. Body width
m. Wingspan

Appendix B

Alternate Ranging Method

An alternate method to calculate the remaining range to go for the vehicle is to extend the integration of the equations of motion to the final part of the trajectory. For this portion of flight the angle of attack is set to 20°, which closely corresponds to the maximum L/D for the vehicle. The initial flight path angle, γ, is set to 15°, and the initial altitude and velocity are 29.4 km and 0.764 km/s (2500 fps), respectively. Range is maximized by setting the bank angle, ϕ, to zero, thereby achieving maximum lift. Integration of the equations of motion subjected to the above constraints yields a range of 82.6 km. The flight profile is shown in Figure 53.

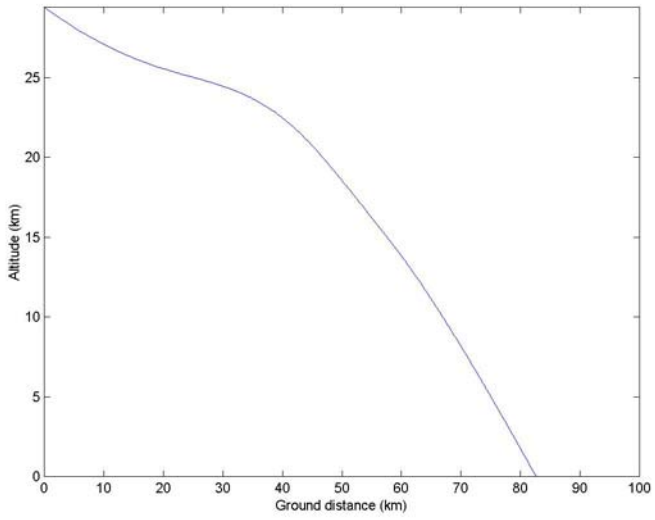

Figure 53: Altitude vs. Distance for Terminal Flight (ϕ=0°)

The constraints above assumed that the vehicle would fly with zero bank angle to maximize range. This will likely not be the case as the vehicle maneuvers into position with the runway for landing. To estimate the range capability in the presence of non-zero bank angle, an average bank angle can be used. This approach allows an estimate of range to be obtained without knowing the terminal flight path in advance. Figure 54 shows the effects of a 30° average bank angle on the range.

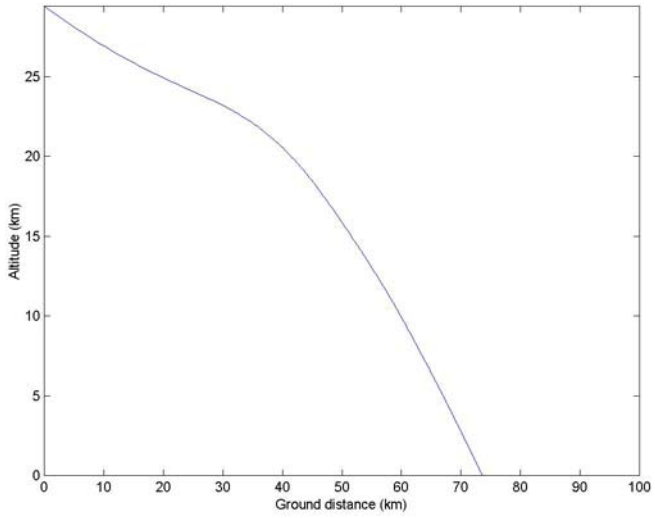

Figure 54: Altitude vs. Distance for Terminal Flight (ϕ_{avg}= 30°)

Appendix C

Initial Lat/Long Determination

Determining the latitude and longitude of the initial reentry interface point is essentially a problem in spherical trigonometry. The first step is to determine the reentry range, R, using Equations 47-49 with the appropriate initial and final conditions for velocity, energy, and drag. Next, the ground trace of the initial orbit is determined and plotted. The final step is to determine the point in the orbit, approaching the landing site, that lies a distance R, or more specifically an angle θ = R/Re, from the landing site. This is accomplished by choosing a longitude at least 180° from the landing site. Then, using the accompanying latitude for the orbit, the range angle between this point and the landing site is determined using:

$$R_{angle} = \cos^{-1}\left[\sin(L)\sin(L_L) + \cos(L)\cos(L_L)\cos(l - l_L)\right] \tag{67}$$

where:

L = Latitude from ground trace

L_L = Latitude of landing site

l = Longitude from ground trace

l_L = Longitude of landing site

If the angle is greater than the desired range angle, then the longitude is incremented and, using the accompanying latitude, the range angle is again calculated. This process is continued until the range angle either equals, or becomes less than, the desired range

angle. The position in the orbit where this occurs defines the latitude and longitude of the initial reentry interface.

Bibliography

Air Force Research Laboratory Space Vehicles Directorate (AFRL/SV). "Space Maneuver Vehicle." n.pag. http://www.vs.afrl.af.mil/Factsheets/smv.html 29 January 2004.

Bate, Roger R. and others. *Fundamentals of Astrodynamics*. New York: Dover Publications, Inc., 1971.

Blanchard, Robert C., Kevin T. Larman, and Christina D. Moats. "Rarefied Flow Shuttle Aerodynamics Flight Model," *Journal of Spacecraft and Rockets*, 31:550-556 (July-August, 1994).

Chapman, Dean R. "On the Corridor and Associated Trajectory Accuracy for Entry of Manned Spacecraft into Planetary Atmospheres," *AIAA Selected Reprint Series*, 1:28-41 (1967).

Dryden Flight Research Center. "X-40A Project Update." n.pag. http://www.dfrc.nasa.gov/Research/X40A.

Harpold, J.C., and C.A. Graves. *Shuttle Entry Guidance*, AAS Paper 78-147, American Astronautical Society, Anniversary Conference, 25th, Houston, Tex., Oct. 30-Nov. 2, 1978.

Lu, Ping. "Entry Guidance and Trajectory Control for Reusable Launch Vehicle," *Journal of Guidance, Control, and Dynamics*, 20:143-149 (January-February 1997).

Marshall Space Flight Center. "X-37 Demonstrator to Test Future Launch Technologies in Orbit and Reentry Environments." n.pag. http://www1.msfc.nasa.gov/NEWSROOM/background/facts/x37. 29 January 2004.

Pratt, Timothy and others. *Satellite Communications*. USA: John Wiley & Sons, Inc., 2003.

Regan, Frank J. and Anandakrishnan, Satya M. *Dynamics of Atmospheric Reentry*. Washington DC: American Institute of Aeronautics and Astronautics, Inc., 1993.

Shaw, M.A., J.L Carlin and J.D. Adams. "Executive Summary of Analyses of the Space Maneuver Vehicle (SMV)." Report to Space and Missile Systems Center Air Force Materiel Command, Los Angeles Air Force Base, CA. September 2000.

-----. "Analyses of the Space Maneuver Vehicle (SMV)." Report to Space and Missile Systems Center Air Force Materiel Command, Los Angeles Air Force Base, CA. September 2000.

South, David J. *Real-Time Optimal Guidance with Application to Lifting Re-entry Vehicles*. Air Force Institute of Technology (AU), Wright-Patterson AFB OH, March 1974 (DS/EE/73-2).

Strang, Gilbert. *Linear Algebra and its Applications*. San Diego: Harcourt Brace Jovanovich, Publishers, 1988.

Tragesser, Steven. Class lecture, MECH 637, Astrodynamic Reentry. Department of Aeronautics and Astronuatics, Air Force Institute of Technology, Wright-Patterson AFB OH, Summer 2003.

Vinh, Nguyen X. and others. *Hypersonic and Planetary Entry Mechanics*. Ann Arbor: The University of Michigan Press, 1980.

Wiesel, William E. *Spaceflight Dynamics*. Boston: The McGraw-Hill Companies, Inc., 1997.

"X-37 Reusable Spaceplane." Excerpt from an unpublished article. n. pag. http://www.boeing.com/phantom/x37. 29 January 2004.

Vita

Dennis John McNabb graduated from Orange Park High School and then attended the University of North Florida for two years. He then transferred to the University of Florida where he graduated in 1997 with the degree of Bachelor of Science in Aerospace Engineering. He then entered the Air Force Officer Training School in March 1998 and was commissioned in June 1998. After completing training at Vandenberg Air Force Base he was assigned to the 45th Range Squadron, Cape Canaveral Air Force Station. In September 2002 he entered the Air Force Institute of Technology where he earned the degree of Master of Science in Astronautical Engineering in March 2004. Upon graduation he was assigned to Detachment 12, Space and Missile Systems Center, Kirtland Air Force Base.

REPORT DOCUMENTATION PAGE

Form Approved
OMB No. 074-0188

1. REPORT DATE *(DD-MM-YYYY)*	2. REPORT TYPE	3. DATES COVERED *(From – To)*
12 Mar 2004	Master's Thesis	Oct 2002 – Mar 2004

4. TITLE AND SUBTITLE

INVESTIGATION OF ATMOSPHERIC REENTRY FOR THE SPACE MANEUVER VEHICLE

5a. CONTRACT NUMBER

5b. GRANT NUMBER

5c. PROGRAM ELEMENT NUMBER

6. AUTHOR(S)

McNabb, Dennis J., Captain, USAF

5d. PROJECT NUMBER

5e. TASK NUMBER

5f. WORK UNIT NUMBER

7. PERFORMING ORGANIZATION NAMES(S) AND ADDRESS(S)

Air Force Institute of Technology
Graduate School of Engineering and Management (AFIT/EN)
2950 Hobson Way, Building 640
WPAFB OH 45433-7765

8. PERFORMING ORGANIZATION REPORT NUMBER

AFIT/GA/ENY/04-M03

9. SPONSORING/MONITORING AGENCY NAME(S) AND ADDRESS(ES)

AFRL/VACD
Thomas H. Jacobs
2180 8th St
WPAFB, OH 45433-7505

10. SPONSOR/MONITOR'S ACRONYM(S)

11. SPONSOR/MONITOR'S REPORT NUMBER(S)

12. DISTRIBUTION/AVAILABILITY STATEMENT

APPROVED FOR PUBLIC RELEASE; DISTRIBUTION UNLIMITED.

13. SUPPLEMENTARY NOTES

14. ABSTRACT

This study investigated the atmospheric reentry of the Space Maneuver Vehicle from low-earth orbit using an entry guidance concept similar to the Space Shuttle. The Space Maneuver Vehicle was modeled as a point mass with aerodynamic properties as determined using Newtonian impact theory. For the rarefied-flow transition regime bridging formulae are used to capture the effects of both hypersonic continuum flow and free molecular flow. Constraints to the reentry are developed and a reentry corridor is defined in the drag-velocity plane. Bank angle modulation is established as the primary means for controlling drag and range. The guidance concept is applied to both a high inclination orbit and a low inclination orbit with crossrange requirement. Monte Carlo error analysis validates the ability of the control algorithm to guide reentry in the presence of initial state errors, as well as atmospheric variations.

15. SUBJECT TERMS

Atmospheric Reentry, Space Maneuver Vehicle, Reentry Guidance, Drag Profile Guidance, Reentry Corridor

16. SECURITY CLASSIFICATION OF:			17. LIMITATION OF ABSTRACT	18. NUMBER OF PAGES	19a. NAME OF RESPONSIBLE PERSON
a. REPORT	b. ABSTRACT	c. THIS PAGE			William E. Wiesel, Civ, USAF
U	U	U	UU	95	19b. TELEPHONE NUMBER *(Include area code)* (937) 255-6565, ext 4312 (William.Wiesel@afit.edu)

Standard Form 298 (Rev. 8-98)
Prescribed by ANSI Std. Z39-18